Intraflagellar transport-A deficiency ameliorates ADPKD renal cystogenesis in a renal tubular- and maturation-dependent manner

Wei Wang[1], Luciane M. Silva[1], Bailey A. Allard[1], Tana S. Pottorf[1], Henry H. Wang[1], Damon T. Jacobs[1], Joseph T. Cornelius[1], Aakriti Chaturvedi[1], Michele T. Pritchard[2], Madhulika Sharma[3], Darren P. Wallace[3], James P. Calvet[4], Pamela V. Tran[1]

[1]Dept. of Anatomy and Cell Biology, The Jared Grantham Kidney Institute, University of Kansas Medical Center, Kansas City, KS

[2]Dept. of Pharmacology, Toxicology and Therapeutics, The Jared Grantham Kidney Institute, University of Kansas Medical Center, Kansas City, KS

[3]Dept. of Internal Medicine, The Jared Grantham Kidney Institute, University of Kansas Medical Center, Kansas City, KS

[4]Dept. of Biochemistry and Molecular Biology, The Jared Grantham Kidney Institute, University of Kansas Medical Center, Kansas City, KS

Running Title: IFT-A dysfunction in ADPKD

Correspondence should be addressed to:

Pamela V. Tran

Department of Anatomy and Cell Biology and

The Jared Grantham Kidney Institute

University of Kansas Medical Center

3901 Rainbow Blvd., MS #3038

Kansas City, KS 66160

Tel: 913-945-7325

Fax: 913-588-2710

E-mail: ptran@kumc.edu

Key Words: mouse models, primary cilia, renal cystic disease, tubule-specific

Abstract

Background: Primary cilia are sensory organelles that are built and maintained by intraflagellar transport (IFT) multi-protein complexes. Deletion of certain ciliary genes in Autosomal Dominant Polycystic Kidney Disease (ADPKD) mouse models markedly attenuates PKD severity, indicating that a component of cilia dysfunction may have critical therapeutic potential.

Method: We have ablated the *Ift-A* gene, *Thm1*, globally in juvenile and adult mouse models of ADPKD.

Results: Relative to juvenile *Pkd2* conditional knock-out mice, deletion of *Thm1* together with *Pkd2* resulted in a complex phenotype, with reduced kidney weight/body weight (KW/BW) ratios, reduced cortical collecting duct-derived cysts, but increased proximal tubular and glomerular dilations, and similar blood urea nitrogen (BUN) levels. Additionally, primary cilia of cortical collecting duct epithelia were lengthened in *Pkd2* conditional knock-out kidneys, as well as in *Pkd2;Thm1* double knock-out kidneys. In contrast, *Thm1* deletion in adult ADPKD mouse models markedly reduced multiple disease parameters, including KW/BW ratios, collecting duct- and loop of Henle-derived cysts, proximal tubular dilations, and BUN levels. Further, primary cilia lengths of cortical collecting duct epithelia were increased in *Pkd1* and *Pkd2* conditional knock-out mice, but similar to control in *Pkd1;Thm1* and *Pkd2;Thm1* double knock-out mice.

Conclusions: These data reveal that during kidney development, *Thm1* both promotes and inhibits different aspects of ADPKD renal cystogenesis in a tubule-dependent manner; however, during adult kidney homeostasis, *Thm1* promotes virtually all features of ADPKD renal cyst growth. These findings suggest that differential factors between tubules and between developing versus mature renal microenvironments influence cilia dysfunction and ADPKD pathobiology.

Introduction

Autosomal Dominant Polycystic Kidney Disease (ADPKD) is among the most common, fatal monogenetic diseases, affecting 1:500 individuals worldwide. ADPKD is characterized by the growth of large fluid-filled renal cysts, which cause injury and fibrosis and can lead to end-stage renal disease by the 6th decade of life. Tolvaptan is the only FDA-approved therapy, but has variable effectiveness[1, 2]. Thus, the need to discover additional underlying disease mechanisms and design new therapeutic strategies continues.

Primary cilia are small, antenna-like sensory organelles that play an important role in ADPKD pathobiology via mechanisms that remain unclear. ADPKD is caused by mutations in *PKD1* (≥80% of cases) or *PKD2* (≥10% of cases), which encode polycystin 1 (PC1) and polycystin 2 (PC2), respectively[3, 4]. PC1 and PC2 form an ion-channel receptor complex that functions at the primary cilium. While PC1 and PC2 also localize to other subcellular compartments, analyses of human ADPKD primary renal epithelial cells, of mouse models harboring human ADPKD mutations, and of an ENU-induced *Pkd2* mouse mutation that causes ciliary exclusion of PC2, indicate that deficiency of PC1 or PC2 from the cilium is sufficient to cause ADPKD[5-7].

Primary cilia are synthesized and maintained via intraflagellar transport (IFT), which is the bi-directional transport of protein cargo along a microtubular axoneme. Two multiprotein complexes mediate IFT. The IFT-B complex interacts with the kinesin motor and mediates anterograde IFT, while the IFT-A complex together with cytoplasmic dynein mediates retrograde IFT. IFT-A proteins are also required for ciliary import of membrane and signaling molecules[8-10]. In mice, deletion of *Ift-A* or *-B* genes either perinatally or in the embryonic kidney results in renal cystic disease[11-13]. However, these mutants differ from ADPKD models in manifesting generally smaller renal cysts and greater fibrosis relative to cyst size[14, 15]. Additionally, *Ift-A* and *–B* mutants differ in cilia phenotype, showing in

general shortened and absent cilia, respectively, and can also show opposing signaling phenotypes, reflecting the differing functional roles of IFT-A and -B[12, 16-18]. Intriguingly, deletion of *Ift-B* genes, *Kif3a*, *Ift20*, and of an IFT-A adaptor gene, *Tulp3*, in *Pkd1* or *Pkd2* conditional knock-out (cko) mice reduces severity of the PKD phenotype[19-21]. The mechanisms underlying this rescue remains elusive, but the impressive attenuation of PKD severity in these *Pkd; cilia* double knock-out (dko) mice indicates that a component of cilia dysfunction has potential critical therapeutic value.

A commonly mutated *IFT* gene is *THM1* (TPR-containing Hedgehog modulator 1; also termed *TTTC21B*). Causative and modifying mutations in *THM1* have been identified in 5% of patients with ciliopathies, including nephronophthisis, Bardet Biedl syndrome, Meckel syndrome and Jeune syndrome[14]. *THM1* encodes an IFT-A component, and its deletion impairs retrograde IFT, causing accumulation of proteins in bulb-like distal tips of shortened primary cilia[16]. *Thm1* loss also impairs cilia entry of membrane-associated proteins, delays and reduces ciliogenesis, and promotes cilia disassembly[22]. In mice, *Thm1* deletion recapitulates many of the clinical manifestations of ciliopathies[16, 23, 24]. Perinatal global deletion of *Thm1* results in renal cystic disease[23]. Deletion of *Thm1* in adult mice does not result in a renal phenotype by 3 months of age, consistent with the developmental time-frame that determines whether loss of a cystogenic gene will cause rapid- or slow-progressing renal cystic disease[25]. Here we have examined the role of IFT-A deficiency in ADPKD by deleting *Thm1* in juvenile and adult ADPKD mouse models. We observe that during postnatal kidney development, *Thm1* loss both attenuates and exacerbates different features of ADPKD, while in the adult kidney, *Thm1* loss markedly attenuates most aspects of ADPKD renal cystogenesis. These data reveal renal tubular- and maturation-dependent roles for IFT-A in ADPKD.

Methods

Generation of mice

Pkd1$^{flox/flox}$, *Pkd2*$^{flox/flox}$ and *ROSA26-Cre* mice were obtained from the Jackson Laboratories (Stock numbers 010671, 017292 and 004847, respectively). Generation of *Thm1* cko mice has been described previously[23]: *Thm1*$^{aln/+}$; *ROSA26Cre*$^{ERT+}$ male mice were mated to *Thm1*$^{flox/flox}$ females. *Pkd1* floxed alleles were introduced into the colony to generate *Thm1*$^{flox/flox}$;*Pkd1*$^{flox/flox}$ or *Thm1*$^{flox/flox}$;*Pkd1*$^{flox/+}$ females and *Pkd1*$^{flox/flox}$; *Thm1*$^{aln/+}$, *ROSA26-Cre*$^{ERT/+}$ males, which were mated. Similarly, *Pkd2* floxed alleles were introduced into the colony to generate *Thm1*$^{flox/flox}$;*Pkd2*$^{flox/flox}$ or *Thm1*$^{flox/flox}$;*Pkd2*$^{flox/+}$ females and *Pkd2*$^{flox/flox}$; *Thm1*$^{aln/+}$, *ROSA26-Cre*$^{ERT/+}$ males. To generate early-onset *Pkd2* models, *Thm1*$^{flox/flox}$;*Pkd2*$^{flox/flox}$ or *Thm1*$^{flox/flox}$;*Pkd2*$^{flox/+}$ nursing mothers mated to *Pkd2*$^{flox/flox}$; *Thm1*$^{aln/+}$, *ROSA26-Cre*$^{ERT/+}$ males were injected intraperitoneally with tamoxifen (10mg/40g; Sigma) at postnatal day 0 (P0) to induce gene deletion. Offspring were analyzed at P21. To generate late-onset *Pkd2* models, offspring from matings between *Thm1*$^{flox/flox}$;*Pkd2*$^{flox/flox}$ or *Thm1*$^{flox/flox}$;*Pkd2*$^{flox/+}$ females and *Pkd2*$^{flox/flox}$; *Thm1*$^{aln/+}$, *ROSA26-Cre*$^{ERT/+}$ males were injected intraperitoneally with tamoxifen (10mg/40g) at P28. To generate late-onset *Pkd1* models, offspring from matings between *Thm1*$^{flox/flox}$;*Pkd1*$^{flox/flox}$ or *Thm1*$^{flox/flox}$;*Pkd1*$^{flox/+}$ females and *Pkd2*$^{flox/flox}$; *Thm1*$^{aln/+}$, *ROSA26-Cre*$^{ERT/+}$ males were injected intraperitoneally with tamoxifen (10mg/40g) at P35. Mice were analyzed at 6 months of age. All mouse lines were maintained on a pure C57BL6/J background (backcrossed 10 generations). All animal procedures were conducted in accordance with KUMC-IACUC and AAALAC rules and regulations.

Kidney and body weight measurements

Kidneys were dissected and weighed using a standard laboratory weighing scale. The KW/BW ratio was calculated as the total kidney weights divided by body weight for each mouse.

Western blot

Passive Lysis Buffer (Promega) containing proteinase inhibitor cocktail (Pierce) was used to generate protein extracts from frozen kidney tissue. Tissue was homogenized by using 0.5 mm zirconium oxide PINK beads (Next Advance) and a Bullet Blender Storm (Next Advance) set at Speed 10 for approximately 5 minutes. Lysates were centrifuged at 4^0C at maximum speed for 1 minute and supernatant was collected. Protein concentrations were determined using the bicinchoninic acid protein (BCA) assay reagents (Pierce). Western blot was performed as described [23], using primary antibodies for P-STAT3 (Cell Signaling Technology, 9145), STAT3 (Cell Signaling Technology, 9139), P-ERK (Cell Signaling Technology, 4370), ERK (Cell Signaling Technology, 4696). SuperSignal West Femto Chemiluminescent Substrate (Pierce) was used to detect signal. ImageJ was used to quantify Western blot signals.

qPCR

RNA was extracted using Trizol (Life Technologies), then reverse transcribed into cDNA using Quanta Biosciences qScript cDNA mix (VWR International). qPCR for *Ccl2* was performed using Quanta Biosciences Perfecta qPCR Supermix (VWR International) in a BioRad CFX Connect Real-Time PCR Detection System. Primers used were *mCcl2* (Forward: 5'-AAGCTCAACCCTGACTTCTTAC-3'; Reverse: 5'-CAACGTCTGAGAACTGGAGAAA-3'). qPCR was performed in duplicate using RNA lysates from five samples per genotype.

Histology

Kidneys were bisected transversely, fixed in 10% formalin for several days, then processed in a tissue processor and embedded in paraffin. Tissue sections (7μm) were obtained with a microtome. Sections were deparaffinized, rehydrated through a series of ethanol washes, and stained with hematoxylin and eosin (H&E). Images were taken with a Nikon 80i microscope equipped with a Nikon DS-Fi1 camera. Cystic areas of H&E-stained sections were quantified using ImageJ.

Immunofluorescence

Following deparaffinization and rehydration, tissue sections were subjected to an antigen retrieval protocol, which consisted of steaming sections for 25 minutes in Sodium Citrate Buffer (10 mM Sodium Citrate, 0.05% Tween 20, pH 6.0). Sections were blocked with 1% BSA in PBS for 1 hour at room temperature, and then incubated with primary antibodies against acetylated-α tubulin (1:4000; Sigma, T7451), IFT81 (1:200; Proteintech, 11744-1-AP), αSMA (1:500; Abcam, ab5694) and PCNA (1:300; Cell Signaling Technology, 13110), DBA (1:100; Vector Laboratories, FL-1031), LTL (1:300, Vector Laboratories, FL-1321), THP (1:100; Santa Cruz Biotechnology, sc-271022) overnight at 4°C. Sections were washed three times in PBS, and then incubated with secondary antibodies conjugated to Alexa Fluor 488 (1:500; Invitrogen, A-11001 (anti-mouse) or A-11034 (anti-rabbit)) or Alexa Fluor 594 (1:500; Invitrogen, A-11005 (anti-mouse) or A-11012 (anti-rabbit)) for 1 hour at room temperature. After three washes of PBS, sections were mounted with Fluoromount-G containing 4′,6-diamidino-2-phenylindole (DAPI) (Electron Microscopy Sciences). Staining was visualized and imaged using a Nikon 80i microscope with a photometrics camera or a Nikon Eclipse TiE attached to an A1R-SHR confocal, with an A1-DU4 detector, and LU4 laser launch.

Blood Urea Nitrogen Measurements

Mouse trunk blood was collected in Microvette CB 300 Blood Collection System tubes (Kent Scientific), and centrifuged at 1800g at room temperature for 10 minutes to collect serum. BUN was measured using the QuantiChrom Urea Assay Kit (BioAssay Systems) according to the manufacturer's protocol.

ADPKD renal sections

Paraffin-embedded sections of de-identified normal human kidney (NHK), n=3 (K357, K402, K419), and of ADPKD, n=3 (K386, K408, K423) were obtained from the PKD Biomaterials Core.

Sections were deparaffinized and rehydrated, steamed in Sodium Citrate Buffer (10 mM Sodium Citrate, 0.05% Tween 20, pH 6.0) for antigen retrieval, and immunostained for ARL13B (1:300; Proteintech, 17711-1-AP).

Statistics

Statistical significance ($P < 0.05$) was determined using either one-way ANOVA followed by Tukey's test, or using an unpaired t-test for comparing more than two groups or two groups, respectively. GraphPad Prism 8 software was used to perform these analyses.

Results

Perinatal deletion of *Thm1* in *Pkd2* cko mice reduces cortical cystogenesis, but does not improve kidney function

To examine the effect of IFT-A deficiency in an early-onset, rapidly progressing ADPKD mouse model, we deleted *Thm1* together with *Pkd2* at postnatal day (P) 0, and examined the renal phenotypes of control, *Thm1* cko, *Pkd2* cko and *Pkd2;Thm1* dko mice at P21. At this stage, *Thm1* cko kidneys appear mostly intact morphologically[23], with some tubular dilations observed in the cortex and with kidney weight/body weight (KW/BW) ratios similar to control (Figures 1A and 1B). Yet, BUN levels are elevated about 2-fold (Figure 1C). In *Pkd2* cko mice, renal cysts are present in both cortex and medulla, and KW/BW ratios and BUN levels are increased 5-fold and 3-fold, respectively. In *Pkd2;Thm1* dko mice, renal cysts are also present in the cortex and medulla, and KW/BW ratios and BUN levels are increased 4-fold and 3-fold, respectively. Thus relative to *Pkd2* cko mice, *Pkd2;Thm1* dko mice have reduced KW/BW ratios, but similar kidney function. *Pkd2;Thm1* dko kidneys also show decreased percent cystic index (Figure 1D, Supplemental Figure 1A), due to reduced cystogenesis in

the cortex (Figure 1E, Supplemental Figure 1B), while percent cystic index in the medulla is similar (Figures 1F and S1C).

Perinatal deletion of *Thm1* in *Pkd2* cko mice reduces cortical collecting duct cystogenesis, but increases proximal tubular and glomerular dilations

Since cystogenesis was reduced in the cortex of *Pkd2;Thm1* dko kidneys relative to *Pkd2* cko kidneys, subsequent analyses focused on the cortex. At P21 in the *Thm1* cko renal cortex, we observed some dilations, most of which were LTL+, marking proximal tubules, and fewer that were THP+ or DBA+, marking loop of Henle and collecting duct, respectively (Figure 2A). In *Pkd2* cko renal cortex, LTL+ dilations, THP+ cysts, and multiple, large DBA+ cysts were observed. In *Pkd2; Thm1* dko cortex, LTL+ dilations were increased relative to those of *Pkd2* cko and *Thm1* cko kidneys (Figures 2A, 2B, Supplemental Figure 1D); THP+ cysts were similar in size to those of *Pkd2* cko kidneys (Figure 2C, Supplemental Figure 1E), and DBA+ cysts were decreased in size relative to those of *Pkd2* cko kidneys (Figure 2D, Supplemental Figure 1F). Thus, we observed a tubular-specific effect of deleting *Thm1* in juvenile *Pkd2* cko mice. *Thm1* deletion worsened LTL+, but attenuated cortical DBA+ cystogenesis.

Histology revealed that glomerular dilations were present across the mutant genotypes (Figure 2E). We observed a reduced number of glomeruli per cross-section in *Pkd2* cko kidneys (28.3 vs 45.0; Supplemental Figure 2B), but a restored number of glomeruli per cross-section in *Pkd2;Thm1* dko kidneys (46.5; Supplemental Figure 2D, Figure 2F). In *Pkd2* cko kidneys, area of Bowman's capsule/area of glomerulus and Bowman's space were increased, suggesting presence of glomerular dilations (Figure 2G, Supplemental Figure 3B). In *Pkd2; Thm1* dko kidneys, these parameters were increased to a greater extent than in *Pkd2* cko kidneys, indicating that additional loss of *Thm1* exacerbates the glomerular dilations caused by loss of *Pkd2* (Figures 2G, 2H, Supplemental Figures 3C and 3D).

Deletion of *Pkd2* increases proliferation of renal tubular epithelia

We next examined cell proliferation, a driver of ADPKD renal cystogenesis, by immunostaining for PCNA together with proximal tubule and collecting duct markers, LTL and DBA, respectively. Similar levels of PCNA staining were observed in normal LTL+ and DBA+ tubules across the various genotypes - control, *Thm1* cko, *Pkd2* cko and *Pkd2;Thm1* dko kidneys (Figures 3A-3B). However, in *Pkd2* cko kidneys, PCNA+ cells were increased in dilated LTL+ tubules relative to normal LTL+ tubules (Supplemental Figure 4), and in *Pkd2* cko and *Pkd2;Thm1* dko kidneys, PCNA+ cells were increased in dilated DBA+ tubules relative to normal DBA+ tubules (Figure 3B). These data support that increased proliferation is an early event in ADPKD renal cystogenesis.

Perinatal deletion of *Thm1* causes fibrosis

Cyst growth compresses surrounding parenchyma, leading to injury and fibrosis in ADPKD. To assess fibrosis, we immunostained kidney sections for presence of myofibroblasts, which label with alpha smooth muscle actin (αSMA). In *Thm1* cko kidneys, we observed αSMA+ cells around glomeruli and tubular dilations (Figure 3C). In *Pkd2* cko kidneys, more αSMA+ labelling was observed than in *Thm1* cko kidneys, and in *Pkd2;Thm1* dko kidneys, levels of αSMA+ labelling were similar to those in *Pkd2* cko kidneys. Thus, deletion of *Thm1* alone causes fibrosis, but *Thm1* deletion in *Pkd2* cko mice does not exacerbate fibrosis at P21.

Perinatal deletion of *Thm1* in *Pkd2* cko mice increases STAT3 signaling

We have observed that perinatal deletion of *Thm1* increases STAT3 activation in kidneys prior to cyst formation (data not shown). STAT3 signaling is also increased in ADPKD mouse models and pharmacological inhibition of STAT3 signaling attenuates ADPKD in mouse models[26]. ERK signaling

is also increased during early cystic kidney disease of *Thm1* cko mice (data not shown) and this pathway is elevated in ADPKD[27, 28]. We therefore examined these pathways using Western blot analyses. In *Thm1* cko and *Pkd2* cko kidneys, STAT3 activation was increased (Figures 4A, Supplemental Figure 5A, Figure 4B, Supplemental Figure 5B), and in *Pkd2;Thm1* dko kidneys, STAT3 activation was further increased (Figures 4B, Supplemental Figures 5C and 5D). Additionally, in *Pkd2* cko and *Pkd2;Thm1* dko kidneys, there was a trend toward increased ERK activation (Figure 4C, Supplemental Figure 6). Thus, *Pkd2* cystic disease causes increased STAT3 and ERK signaling consistent with previous reports[29, 30], and deletion of *Thm1* in *Pkd2* cko mice further increases STAT3 activation.

Deletion of *Pkd2* increases cilia length on renal epithelia

We examined cilia length on renal tubular epithelia by co-immunostaining for acetylated, α-tubulin together with lectins, LTL and DBA. In control kidneys, average cilia lengths were 3.0μm and 2.1μm for LTL+ and DBA+ cells, respectively (Figures 5A and 5B). We also noted qualitative differences between LTL+ and DBA+ primary cilia, with the former cilia appearing thinner and longer, and the latter being thicker and more rod-like. Cilia lengths were increased in both *Pkd2* cko LTL+ and DBA+ tubules. However, relative to *Pkd2* cko tubules, cilia lengths were further increased in *Pkd2;Thm1* dko LTL+ tubules, but similar in *Pkd2;Thm1* dko DBA+ tubules. These differences reveal tubular-specific effects on cilia length.

Deletion of *Thm1* in adult *Pkd2* or *Pkd1* cko mice markedly attenuates ADPKD renal cystogenesis

We next examined the effect of IFT-A deficiency in late-onset, slowly progressive adult ADPKD mouse models. We deleted *Thm1* together with *Pkd2* at P28 and examined the renal

phenotypes of control, *Thm1* cko, *Pkd2* cko and *Pkd2;Thm1* dko mice at 6 months of age. *Thm1* cko kidneys have similar morphology and BUN levels to those of control mice (Supplemental Figures 7A and 7B). *Pkd2* cko mice show renal cysts mostly in the cortex, with the largest cysts being DBA+, and smaller cysts being LTL+ or THP+ (Figure 6A). In contrast, in *Pkd2;Thm1* dko mice, the *Pkd2* cko cystic phenotype is largely corrected morphologically. KW/BW ratios are unchanged in *Pkd2* cko mice, reflecting the mild disease induced in adulthood. BUN levels show a trend toward a slight elevation in *Pkd2* cko mice, but the average BUN value is still within the range of normal renal function. BUN levels of *Pkd2;Thm1* dko mice were similar to those of *Pkd2* cko mice. In ADPKD, pro-inflammatory cytokines, such as *Ccl2*, are elevated[31]. In *Pkd2* cko kidney extracts, expression of *Ccl2* showed an increasing trend, while in *Pkd2; Thm1* dko extract, *Ccl2* levels were similar to control, suggesting reduced inflammation (Supplemental Figure 8A).

We also deleted *Thm1* together with *Pkd1* at P35 and examined the renal phenotypes at 6 months of age. *Thm1* cko kidneys have morphology resembling control kidneys (Supplemental Figure 7C), similar to *Thm1* deletion at P28. Like *Pkd2* cko adult models, *Pkd1* cko renal cysts were mostly in the cortex, with the largest and most abundant cysts being DBA+. Fewer cysts were THP+, and only dilations, not cysts, were observed that were LTL+ (Figure 7A). Notably, all these features were reduced in *Pkd1; Thm1* dko kidneys. KW/BW ratios were elevated in *Pkd1* cko mice, and corrected in *Pkd1;Thm1* dko mice (Figure 7B). Additionally, BUN levels were elevated in *Pkd1* cko mice, although the average value was still within the range of normal kidney function, while BUN levels in *Pkd1;Thm1* dko mice were similar to control. Further, while expression of *Ccl2*, and activation of STAT3 and ERK were increased in kidney extracts of *Pkd1* cko mice, these parameters were normalized in kidneys of *Pkd1; Thm1* dko mice, consistent with attenuation of disease severity (Supplemental Figures 8B-8D).

Cilia length is increased on cortical renal epithelia of mouse and human ADPKD kidneys

We examined cilia length on renal tubular epithelia of adult ADPKD mouse models by co-immunostaining for acetylated, α-tubulin together with DBA. Similar to juvenile ADPKD models, cilia lengths were increased in *Pkd1* cko and *Pkd2* cko DBA+ adult tubules. However, in contrast to juvenile models, cilia lengths were normalized in *Pkd1;Thm1* and *Pkd2;Thm1* dko DBA+ tubules (Figures 8A and 8B). These differences suggest maturation-dependent effects on cilia length.

Further, we examined cilia lengths on renal cortical sections of normal human kidney (NHK) and ADPKD samples. Human ADPKD sections had longer cilia than NHK sections (Figure 8C), suggesting that increased cilia length is also a feature of the human disease.

Discussion

This study demonstrates differential effects of IFT-A deficiency in early- versus late-onset ADPKD mouse models, highlighting differences in developing versus mature renal microenvironments. These data also show that deleting *Thm1* in an early-onset ADPKD model has tubule-specific effects: partially protecting cortical collecting duct structure, but worsening the decline of proximal tubular structural integrity; and restoring glomerular number, but increasing glomerular dilation.

In *Pkd2;Thm1* dko juvenile mice, STAT3 activation was increased. Since cortical collecting duct cystogenesis was reduced, this suggests that STAT3 signaling may contribute to other disease processes. *Pkd2;Thm1* dko kidneys showed increased proximal tubular and glomerular dilations, and increased STAT3 activation could potentially drive these dilations. STAT3 signaling may also be involved in fibrosis. However, while STAT3 activation was increased in *Pkd2;Thm1* dko mice, fibrosis as assessed by αSMA staining was not. In contrast to studies suggesting a pathogenic role for increased STAT3 signaling, a recent study has shown that tubular STAT3 activation restricts immune

cell infiltration in *Pkd1* cko mice[32]. Genetic deletion of *Stat3* together with *Pkd1* in renal tubular cells slightly reduced cystic burden, but did not ameliorate kidney function and increased interstitial inflammation. Thus, STAT3 activation in *Pkd2;Thm1* dko mice could potentially serve a protective role against inflammation.

In several ADPKD mouse models, *PKD1*$^{RC/RC}$, *Pkd1* and *Pkd2* cko mice, renal primary cilia are lengthened[33, 34]. Our data showing increased cilia length in both *Pkd2* juvenile and adult mouse models and in *Pkd1* adult mouse models are consistent with these studies. Additionally, the increased cilia length in ADPKD tissue sections suggest that similar ciliary mechanisms may be relevant to the human disease. We observed a range of cilia lengths within a genotype. This could result from limitations of quantifying immunostained tissue sections. Additionally, multiple factors influence renal cilia length and could also contribute to this variability. Our data suggest that in addition to genotype, cilia length varied by renal tubule and age, suggesting that factors within a tubule's microenvironment affect cilia length. Cilia length is determined by the ratio of cilia assembly and disassembly. As well, intracellular Ca^{2+} and cAMP, oxidative stress, cytokines, and fluid flow influence ciliary length of renal epithelial cells[35-37]. These multiple factors indicate that cilia length regulation may be fine-tuned in order to maintain renal tubular structure and function. In support of this, genetic and pharmacological inhibition of cilia disassembly in *Pkd1* cko mice increased renal cilia length and exacerbated ADPKD[38]. In the *jck* non-orthologous ADPKD mouse model, renal primary cilia are also lengthened, and pharmacological shortening of primary cilia in *jck* mutant mice was associated with an attenuation of the ADPKD phenotype[19, 39]. Moreover, cilia length is altered also in acute kidney injury and chronic kidney disease[40-43]. Thus, to understand mechanisms of renal tubule homeostasis, the connections between cilia length and cilia function, and renal disease require deeper study.

Thus far, the effects of deleting Ift-B genes, *Kif3a* and *Ift20*, and of the IFT-A adaptor, *Tulp3*, in ADPKD mouse models have been demonstrated. Ift-B gene deletion attenuates PKD severity in both tubular-specific juvenile and adult models of ADPKD[19]. In contrast, *Tulp3* deletion did not rescue

renal cystic disease in a tubular-specific juvenile model of ADPKD, but did in an adult model[21, 44]. Similarly, global deletion of *Thm1* in a juvenile ADPKD model results in a complex phenotype, but in an adult model, rescues most aspects of the renal cystic disease. Perinatal loss of *Thm1* results in cystic kidney disease[23], indicating that *Thm1* is required for kidney maturation, which might account for the lack of rescue in juvenile models. However, perinatal deletion of *Kif3a* and mutation of *Tulp3* also causes renal cystic disease[21, 45], suggesting these genes are required as well for kidney differentiation and maturation. Thus, there may be functional differences between IFT-B and IFT-A and *Tulp3* that result in attenuated disease in juvenile *Pkd;Ift-B* dko mice, but not in *Pkd;Thm1* or *Pkd;Tulp3* dko mice. These differences could include differential roles in IFT, cilia length regulation, and/or ciliary-mediated signaling. For instance, *Ift-B* genes are required for anterograde IFT, unlike *Thm1* and *Tulp3*. While IFT-B and IFT-A regulate cilia length, a role for *Tulp3* in altering cilia length has not been reported. Further, IFT-B and IFT-A mutants have shown opposing signaling phenotypes.

We noted that in the late-onset models, BUN levels were similar between *Pkd2* cko and *Pkd2;Thm1* dko mice, while in contrast, BUN levels in *Pkd1;Thm1* dko mice were reduced relative to those of *Pkd1* cko mice, suggesting *Thm1* deletion might confer greater protection in *Pkd1* cko mice than in *Pkd2* cko mice. We deleted *Pkd2* one week earlier than *Pkd1*, since *Pkd1* deficiency results in a more severe ADPKD phenotype than *Pkd2* deficiency. Importantly, *Thm1* deletion at P28 resulted in BUN levels similar to those of control mice at 6 months of age, and *Thm1* deletion at either P28 or P35 resulted in kidney morphology resembling control. Thus, the BUN data may suggest a functional difference between *Pkd2;Thm1* dko and *Pkd1;Thm1* dko mice.

The mechanisms by which *Pkd; cilia* dko mice attenuate ADPKD severity are still obscure. Reducing *Ccl2* signaling and altering lipid composition of the ciliary membrane have been proposed[20, 21, 44]. Primary cilia are designed to detect both chemical and mechanical cues in the extracellular environment. While mechanosensing by primary cilia and the polycystins has been controversial, recent studies have renewed interest in a potential mechanosensory role for the polycystins,

particularly regarding tissue microenvironment stiffness[46, 47]. If sensing physical forces in the tissue microenvironment is essential to maintaining renal tubular function, then other mechanical cues that would change with cyst growth include shear stress and intraluminal pressure. Cilia length could then also be a possible contributing factor in PKD severity. Further, by extrapolating findings of cilia studies from the cancer field[48], cilia of not only renal tubular epithelial cells, but of interstitial cells might also affect signaling and disease severity.

In summary, our data demonstrate for the first time the role of IFT-A in an ADPKD context in developing versus mature kidneys. Defining the mechanisms by which IFT-A deficiency attenuates ADPKD in adult models will be critical to identifying potential therapeutic targets.

Acknowledgements

We thank members of the KUMC Dept. of Anatomy and Cell Biology and the Jared Grantham Kidney Institute for helpful discussions. We thank Jing Huang of the KUMC Histology Core and acknowledge support of this core (Intellectual and Developmental Disabilities Research Center NIH U54 HD090216; COBRE NIH P30 GM122731). This work was also supported by a K-INBRE Summer Student Award to JTC [K-INBRE P20GM103418] and the National Institutes of Health (P20 GM14936; P30DK106912; R01DK108433 to MS; R01DK103033 to PVT).

Disclosures

The authors declare no conflict of interest.

Contributions

WW, LMS, BAA, TSP, HHW, DTJ, JTC, AC, MTP, MS, DPW, and PVT performed experiments.

WW, LMS, BAA, TSP, HHW, DTJ, JTC, AC, MTP, MS, DPW, JPC and PVT analyzed and

interpreted data. WW, LMS, BAA, and PVT designed research. WW, LMS, and PVT wrote the manuscript.

References

1. Torres, VE, Chapman, AB, Devuyst, O, Gansevoort, RT, Grantham, JJ, Higashihara, E, Perrone, RD, Krasa, HB, Ouyang, J, Czerwiec, FS: Tolvaptan in patients with autosomal dominant polycystic kidney disease. *N Engl J Med*, 367**:** 2407-2418, 2012.
2. Blair, HA: Tolvaptan: A Review in Autosomal Dominant Polycystic Kidney Disease. *Drugs*, 2019.
3. Torres, VE, Harris, PC: Mechanisms of Disease: autosomal dominant and recessive polycystic kidney diseases. *Nat Clin Pract Nephrol*, 2**:** 40-55; quiz 55, 2006.
4. Porath, B, Gainullin, VG, Cornec-Le Gall, E, Dillinger, EK, Heyer, CM, Hopp, K, Edwards, ME, Madsen, CD, Mauritz, SR, Banks, CJ, Baheti, S, Reddy, B, Herrero, JI, Banales, JM, Hogan, MC, Tasic, V, Watnick, TJ, Chapman, AB, Vigneau, C, Lavainne, F, Audrezet, MP, Ferec, C, Le Meur, Y, Torres, VE, Genkyst Study Group, HPoPKDG, Consortium for Radiologic Imaging Studies of Polycystic Kidney, D, Harris, PC: Mutations in GANAB, Encoding the Glucosidase IIalpha Subunit, Cause Autosomal-Dominant Polycystic Kidney and Liver Disease. *Am J Hum Genet*, 98**:** 1193-1207, 2016.
5. Freedman, BS, Lam, AQ, Sundsbak, JL, Iatrino, R, Su, X, Koon, SJ, Wu, M, Daheron, L, Harris, PC, Zhou, J, Bonventre, JV: Reduced ciliary polycystin-2 in induced pluripotent stem cells from polycystic kidney disease patients with PKD1 mutations. *J Am Soc Nephrol*, 24**:** 1571-1586, 2013.
6. Cai, Y, Fedeles, SV, Dong, K, Anyatonwu, G, Onoe, T, Mitobe, M, Gao, JD, Okuhara, D, Tian, X, Gallagher, AR, Tang, Z, Xie, X, Lalioti, MD, Lee, AH, Ehrlich, BE, Somlo, S: Altered trafficking and stability of polycystins underlie polycystic kidney disease. *J Clin Invest*, 124**:** 5129-5144, 2014.
7. Walker, RV, Keynton, JL, Grimes, DT, Sreekumar, V, Williams, DJ, Esapa, C, Wu, D, Knight, MM, Norris, DP: Ciliary exclusion of Polycystin-2 promotes kidney cystogenesis in an autosomal dominant polycystic kidney disease model. *Nature communications*, 10**:** 4072, 2019.
8. Fu, W, Wang, L, Kim, S, Li, J, Dynlacht, BD: Role for the IFT-A Complex in Selective Transport to the Primary Cilium. *Cell reports*, 17**:** 1505-1517, 2016.
9. Mukhopadhyay, S, Wen, X, Chih, B, Nelson, CD, Lane, WS, Scales, SJ, Jackson, PK: TULP3 bridges the IFT-A complex and membrane phosphoinositides to promote trafficking of G protein-coupled receptors into primary cilia. *Genes Dev*, 24**:** 2180-2193, 2010.
10. Liem, KF, Jr., Ashe, A, He, M, Satir, P, Moran, J, Beier, D, Wicking, C, Anderson, KV: The IFT-A complex regulates Shh signaling through cilia structure and membrane protein trafficking. *J Cell Biol*, 197**:** 789-800, 2012.
11. Yoder, BK, Tousson, A, Millican, L, Wu, JH, Bugg, CE, Jr., Schafer, JA, Balkovetz, DF: Polaris, a protein disrupted in orpk mutant mice, is required for assembly of renal cilium. *American journal of physiology Renal physiology*, 282**:** F541-552, 2002.
12. Jonassen, JA, SanAgustin, J, Baker, SP, Pazour, GJ: Disruption of IFT complex A causes cystic kidneys without mitotic spindle misorientation. *J Am Soc Nephrol*, 23**:** 641-651, 2012.
13. Lin, F, Hiesberger, T, Cordes, K, Sinclair, AM, Goldstein, LS, Somlo, S, Igarashi, P: Kidney-specific inactivation of the KIF3A subunit of kinesin-II inhibits renal ciliogenesis and produces polycystic kidney disease. *Proc Natl Acad Sci U S A*, 100**:** 5286-5291, 2003.
14. Davis, EE, Zhang, Q, Liu, Q, Diplas, BH, Davey, LM, Hartley, J, Stoetzel, C, Szymanska, K, Ramaswami, G, Logan, CV, Muzny, DM, Young, AC, Wheeler, DA, Cruz, P, Morgan, M, Lewis, LR, Cherukuri, P, Maskeri, B, Hansen, NF, Mullikin, JC, Blakesley, RW, Bouffard,

GG, Program, NCS, Gyapay, G, Rieger, S, Tonshoff, B, Kern, I, Soliman, NA, Neuhaus, TJ, Swoboda, KJ, Kayserili, H, Gallagher, TE, Lewis, RA, Bergmann, C, Otto, EA, Saunier, S, Scambler, PJ, Beales, PL, Gleeson, JG, Maher, ER, Attie-Bitach, T, Dollfus, H, Johnson, CA, Green, ED, Gibbs, RA, Hildebrandt, F, Pierce, EA, Katsanis, N: TTC21B contributes both causal and modifying alleles across the ciliopathy spectrum. *Nat Genet,* 43**:** 189-196, 2011.

15. Srivastava, S, Molinari, E, Raman, S, Sayer, JA: Many Genes-One Disease? Genetics of Nephronophthisis (NPHP) and NPHP-Associated Disorders. *Front Pediatr,* 5**:** 287, 2017.
16. Tran, PV, Haycraft, CJ, Besschetnova, TY, Turbe-Doan, A, Stottmann, RW, Herron, BJ, Chesebro, AL, Qiu, H, Scherz, PJ, Shah, JV, Yoder, BK, Beier, DR: THM1 negatively modulates mouse sonic hedgehog signal transduction and affects retrograde intraflagellar transport in cilia. *Nat Genet,* 40**:** 403-410, 2008.
17. Qin, J, Lin, Y, Norman, RX, Ko, HW, Eggenschwiler, JT: Intraflagellar transport protein 122 antagonizes Sonic Hedgehog signaling and controls ciliary localization of pathway components. *Proceedings of the National Academy of Sciences of the United States of America,* 108**:** 1456-1461, 2011.
18. Eggenschwiler, JT, Anderson, KV: Cilia and developmental signaling. *Annual review of cell and developmental biology,* 23**:** 345-373, 2007.
19. Ma, M, Tian, X, Igarashi, P, Pazour, GJ, Somlo, S: Loss of cilia suppresses cyst growth in genetic models of autosomal dominant polycystic kidney disease. *Nat Genet,* 45**:** 1004-1012, 2013.
20. Viau, A, Bienaime, F, Lukas, K, Todkar, AP, Knoll, M, Yakulov, TA, Hofherr, A, Kretz, O, Helmstadter, M, Reichardt, W, Braeg, S, Aschman, T, Merkle, A, Pfeifer, D, Dumit, VI, Gubler, MC, Nitschke, R, Huber, TB, Terzi, F, Dengjel, J, Grahammer, F, Kottgen, M, Busch, H, Boerries, M, Walz, G, Triantafyllopoulou, A, Kuehn, EW: Cilia-localized LKB1 regulates chemokine signaling, macrophage recruitment, and tissue homeostasis in the kidney. *EMBO J,* 37, 2018.
21. Legue, E, Liem, KF, Jr.: Tulp3 Is a Ciliary Trafficking Gene that Regulates Polycystic Kidney Disease. *Curr Biol,* 29**:** 803-812 e805, 2019.
22. Wang, W, Allard, BA, Pottorf, TS, Wang, HH, Vivian, JL, Tran, PV: Genetic interaction of mammalian IFT-A paralogs regulates cilia disassembly, ciliary entry of membrane protein, Hedgehog signaling, and embryogenesis. *FASEB J,* 2020.
23. Tran, PV, Talbott, GC, Turbe-Doan, A, Jacobs, DT, Schonfeld, MP, Silva, LM, Chatterjee, A, Prysak, M, Allard, BA, Beier, DR: Downregulating hedgehog signaling reduces renal cystogenic potential of mouse models. *J Am Soc Nephrol,* 25**:** 2201-2212, 2014.
24. Jacobs, DT, Silva, LM, Allard, BA, Schonfeld, MP, Chatterjee, A, Talbott, GC, Beier, DR, Tran, PV: Dysfunction of intraflagellar transport-A causes hyperphagia-induced obesity and metabolic syndrome. *Dis Model Mech,* 9**:** 789-798, 2016.
25. Piontek, K, Menezes, LF, Garcia-Gonzalez, MA, Huso, DL, Germino, GG: A critical developmental switch defines the kinetics of kidney cyst formation after loss of Pkd1. *Nat Med,* 13**:** 1490-1495, 2007.
26. Takakura, A, Nelson, EA, Haque, N, Humphreys, BD, Zandi-Nejad, K, Frank, DA, Zhou, J: Pyrimethamine inhibits adult polycystic kidney disease by modulating STAT signaling pathways. *Hum Mol Genet,* 20**:** 4143-4154, 2011.
27. Yamaguchi, T, Pelling, JC, Ramaswamy, NT, Eppler, JW, Wallace, DP, Nagao, S, Rome, LA, Sullivan, LP, Grantham, JJ: cAMP stimulates the in vitro proliferation of renal cyst epithelial cells by activating the extracellular signal-regulated kinase pathway. *Kidney Int,* 57**:** 1460-1471, 2000.
28. Yamaguchi, T, Nagao, S, Wallace, DP, Belibi, FA, Cowley, BD, Pelling, JC, Grantham, JJ: Cyclic AMP activates B-Raf and ERK in cyst epithelial cells from autosomal-dominant polycystic kidneys. *Kidney Int,* 63**:** 1983-1994, 2003.

29. Bhunia, AK, Piontek, K, Boletta, A, Liu, L, Qian, F, Xu, PN, Germino, FJ, Germino, GG: PKD1 induces p21(waf1) and regulation of the cell cycle via direct activation of the JAK-STAT signaling pathway in a process requiring PKD2. *Cell*, 109**:** 157-168, 2002.
30. Shibazaki, S, Yu, Z, Nishio, S, Tian, X, Thomson, RB, Mitobe, M, Louvi, A, Velazquez, H, Ishibe, S, Cantley, LG, Igarashi, P, Somlo, S: Cyst formation and activation of the extracellular regulated kinase pathway after kidney specific inactivation of Pkd1. *Hum Mol Genet*, 17**:** 1505-1516, 2008.
31. Zheng, D, Wolfe, M, Cowley, BD, Jr., Wallace, DP, Yamaguchi, T, Grantham, JJ: Urinary excretion of monocyte chemoattractant protein-1 in autosomal dominant polycystic kidney disease. *J Am Soc Nephrol*, 14**:** 2588-2595, 2003.
32. Viau, A, Baaziz, M, Aka, A, Mazloum, M, Nguyen, C, Kuehn, EW, Terzi, F, Bienaime, F: Tubular STAT3 Limits Renal Inflammation in Autosomal Dominant Polycystic Kidney Disease. *J Am Soc Nephrol*, 2020.
33. Hopp, K, Ward, CJ, Hommerding, CJ, Nasr, SH, Tuan, HF, Gainullin, VG, Rossetti, S, Torres, VE, Harris, PC: Functional polycystin-1 dosage governs autosomal dominant polycystic kidney disease severity. *J Clin Invest*, 122**:** 4257-4273, 2012.
34. Smith, LA, Bukanov, NO, Husson, H, Russo, RJ, Barry, TC, Taylor, AL, Beier, DR, Ibraghimov-Beskrovnaya, O: Development of polycystic kidney disease in juvenile cystic kidney mice: insights into pathogenesis, ciliary abnormalities, and common features with human disease. *J Am Soc Nephrol*, 17**:** 2821-2831, 2006.
35. Besschetnova, TY, Kolpakova-Hart, E, Guan, Y, Zhou, J, Olsen, BR, Shah, JV: Identification of signaling pathways regulating primary cilium length and flow-mediated adaptation. *Curr Biol*, 20**:** 182-187, 2010.
36. Kim, JI, Kim, J, Jang, HS, Noh, MR, Lipschutz, JH, Park, KM: Reduction of oxidative stress during recovery accelerates normalization of primary cilia length that is altered after ischemic injury in murine kidneys. *Am J Physiol Renal Physiol*, 304**:** F1283-1294, 2013.
37. Upadhyay, VS, Muntean, BS, Kathem, SH, Hwang, JJ, Aboualaiwi, WA, Nauli, SM: Roles of dopamine receptor on chemosensory and mechanosensory primary cilia in renal epithelial cells. *Front Physiol*, 5**:** 72, 2014.
38. Nikonova, AS, Plotnikova, OV, Serzhanova, V, Efimov, A, Bogush, I, Cai, KQ, Hensley, HH, Egleston, BL, Klein-Szanto, A, Seeger-Nukpezah, T, Golemis, EA: Nedd9 restrains renal cystogenesis in Pkd1-/- mice. *Proc Natl Acad Sci U S A*, 111**:** 12859-12864, 2014.
39. Husson, H, Moreno, S, Smith, LA, Smith, MM, Russo, RJ, Pitstick, R, Sergeev, M, Ledbetter, SR, Bukanov, NO, Lane, M, Zhang, K, Billot, K, Carlson, G, Shah, J, Meijer, L, Beier, DR, Ibraghimov-Beskrovnaya, O: Reduction of ciliary length through pharmacologic or genetic inhibition of CDK5 attenuates polycystic kidney disease in a model of nephronophthisis. *Hum Mol Genet*, 25**:** 2245-2255, 2016.
40. Verghese, E, Weidenfeld, R, Bertram, JF, Ricardo, SD, Deane, JA: Renal cilia display length alterations following tubular injury and are present early in epithelial repair. *Nephrol Dial Transplant*, 23**:** 834-841, 2008.
41. Verghese, E, Ricardo, SD, Weidenfeld, R, Zhuang, J, Hill, PA, Langham, RG, Deane, JA: Renal primary cilia lengthen after acute tubular necrosis. *J Am Soc Nephrol*, 20**:** 2147-2153, 2009.
42. Han, SJ, Jang, HS, Seu, SY, Cho, HJ, Hwang, YJ, Kim, JI, Park, KM: Hepatic ischemia/reperfusion injury disrupts the homeostasis of kidney primary cilia via oxidative stress. *Biochim Biophys Acta Mol Basis Dis*, 1863**:** 1817-1828, 2017.
43. Park, KM: Can Tissue Cilia Lengths and Urine Cilia Proteins Be Markers of Kidney Diseases? *Chonnam Med J*, 54**:** 83-89, 2018.

44. Hwang, SH, Somatilaka, BN, Badgandi, H, Palicharla, VR, Walker, R, Shelton, JM, Qian, F, Mukhopadhyay, S: Tulp3 Regulates Renal Cystogenesis by Trafficking of Cystoproteins to Cilia. *Curr Biol*, 29**:** 790-802 e795, 2019.
45. Patel, V, Li, L, Cobo-Stark, P, Shao, X, Somlo, S, Lin, F, Igarashi, P: Acute kidney injury and aberrant planar cell polarity induce cyst formation in mice lacking renal cilia. *Hum Mol Genet*, 17**:** 1578-1590, 2008.
46. Cruz, NM, Song, X, Czerniecki, SM, Gulieva, RE, Churchill, AJ, Kim, YK, Winston, K, Tran, LM, Diaz, MA, Fu, H, Finn, LS, Pei, Y, Himmelfarb, J, Freedman, BS: Organoid cystogenesis reveals a critical role of microenvironment in human polycystic kidney disease. *Nat Mater*, 16**:** 1112-1119, 2017.
47. Nigro, EA, Distefano, G, Chiaravalli, M, Matafora, V, Castelli, M, Pesenti Gritti, A, Bachi, A, Boletta, A: Polycystin-1 Regulates Actomyosin Contraction and the Cellular Response to Extracellular Stiffness. *Scientific reports*, 9**:** 16640, 2019.
48. Kiseleva, AA, Korobeynikov, VA, Nikonova, AS, Zhang, P, Makhov, P, Deneka, AY, Einarson, MB, Serebriiskii, IG, Liu, H, Peterson, JR, Golemis, EA: Unexpected Activities in Regulating Ciliation Contribute to Off-target Effects of Targeted Drugs. *Clin Cancer Res*, 25**:** 4179-4193, 2019.

Figure Legends

Figure 1. Juvenile *Pkd2;Thm1* dko mice have reduced cortical cystic index, but not improved kidney function relative to *Pkd2* cko mice. (A) Haemotoxylin and eosin staining of P21 kidney sections. Scale bar - 500μm (B) 2KW/BW ratios (C) BUN levels (D) Percent cystic index (E) Percent cortical cystic index (F) Percent medullary cystic index. *Pkd2* cko percent cystic indices are set at 1. Bars represent mean ± SD. In (B) and (C), statistical significance was determined by one-way ANOVA followed by Tukey's test. *p<0.05; ***p<0.0005; ****p<0.00005. In (E) and (F), statistical significance was determined by unpaired two-tailed t-test. **p<0.005

Figure 2. Early onset *Pkd2; Thm1* dko mice have reduced cortical collecting duct cysts, but increased proximal tubule dilations. (A) Staining of kidney cortex with LTL, THP and DBA. Scale bar - 100μm (B) Percent LTL+ dilations (C) Percent THP+ cystic index (D) Percent DBA+ cystic index in renal cortex. *Pkd2* cko percent cystic indices are set at 1. Bars represent mean ± SD. Statistical significance was determined by unpaired two-tailed t-test. *p<0.05; **p<0.005. (E) Haemotoxylin and eosin staining. Scale bar - 50μm (F) Number of glomeruli (G) Area of Bowman's capsule/area of glomerulus (H) Area of Bowman's space. Bars represent mean ± SD. Statistical significance was determined by one-way ANOVA followed by Tukey's test. **p<0.005; ****p<0.00005

Figure 3. Early onset *Pkd2* cko mice show increased proliferation in dilated cortical collecting ducts. (A) Immunostaining of kidney cortex for PCNA (red) together with LTL or DBA (green). Scale bar - 10μm (B) Percent PCNA+ cells per tubule. Bars represent mean ± SD. Statistical significance was determined by two-way ANOVA followed by Tukey's test. *p<0.05. Note: Control and *Thm1* cko

LTL+ dilations, control DBA+ dilations, and control and *Thm1* cko DBA+ cysts were not observed in sections analyzed. (C) Immunostaining of kidney cortex for αSMA (red). Scale bar - 50μm.

Figure 4. Early onset *Pkd2; Thm1* dko kidneys have increased STAT3 activation. (A) Western blot analysis of kidney extracts. (B) Quantification of P-STAT3/STAT3 and (C) P-ERK/ERK. Statistical significance was determined by one-way ANOVA followed by Tukey's test. *p<0.05; **p<0.005

Figure 5. *Pkd2* cko mice have longer renal epithelial primary cilia. (A) Immunostaining of kidney cortex for acetylated α-tubulin (red) together with LTL (green). Scale bar - 10μm. Quantification of cilia length of LTL+ cells. (B) Immunostaining of kidney cortex for acetylated α-tubulin together with DBA. Scale bar - 10μm. Quantification of cilia length of cortical DBA+ cells. Bars represent mean ± SD. Statistical significance was determined by one-way ANOVA followed by Tukey's test. *p<0.05; ****p<0.00005

Figure 6. *Thm1* deletion rescues ADPKD in late-onset *Pkd2* model. (A) Histology and immunostaining of kidney sections for LTL, THP and DBA. Scale bar - 100μm (B) KW/BW ratios (C) BUN levels. Bars represent mean ± SD. Statistical significance was determined by one-way ANOVA followed by Tukey's test. **p<0.005

Figure 7. *Thm1* deletion rescues ADPKD in late-onset *Pkd1* model. (A) Histology and immunostaining of kidney sections for LTL, THP and DBA. Scale bar - 100μm. (B) KW/BW ratios (C) BUN levels. Bars represent mean ± SD. Statistical significance was determined by one-way

ANOVA followed by Tukey's test. *p<0.05; **p<0.005

Figure 8. Cilia length is increased on cortical renal epithelial cells of mouse and human ADPKD kidneys. (A) Immunostaining for acetylated α-tubulin together with DBA of *Pkd1* cko kidney cortex, and quantification of cilia lengths. Scale bar - 10μm. (B) Immunostaining for acetylated α-tubulin together with DBA of *Pkd2* cko kidney cortex, and quantification of cilia lengths. Scale bar - 10μm. (C) Immunostaining for ARL13B of normal human kidney (NHK) and ADPKD renal sections. Scale bar - 10μm. Quantification of cilia length. Bars represent mean ± SD. Statistical significance was determined by one-way ANOVA followed by Tukey's test. *p<0.05; **p<0.005; ***p<0.0005; ****p<0.00005

Supplemental Material

Fig 1

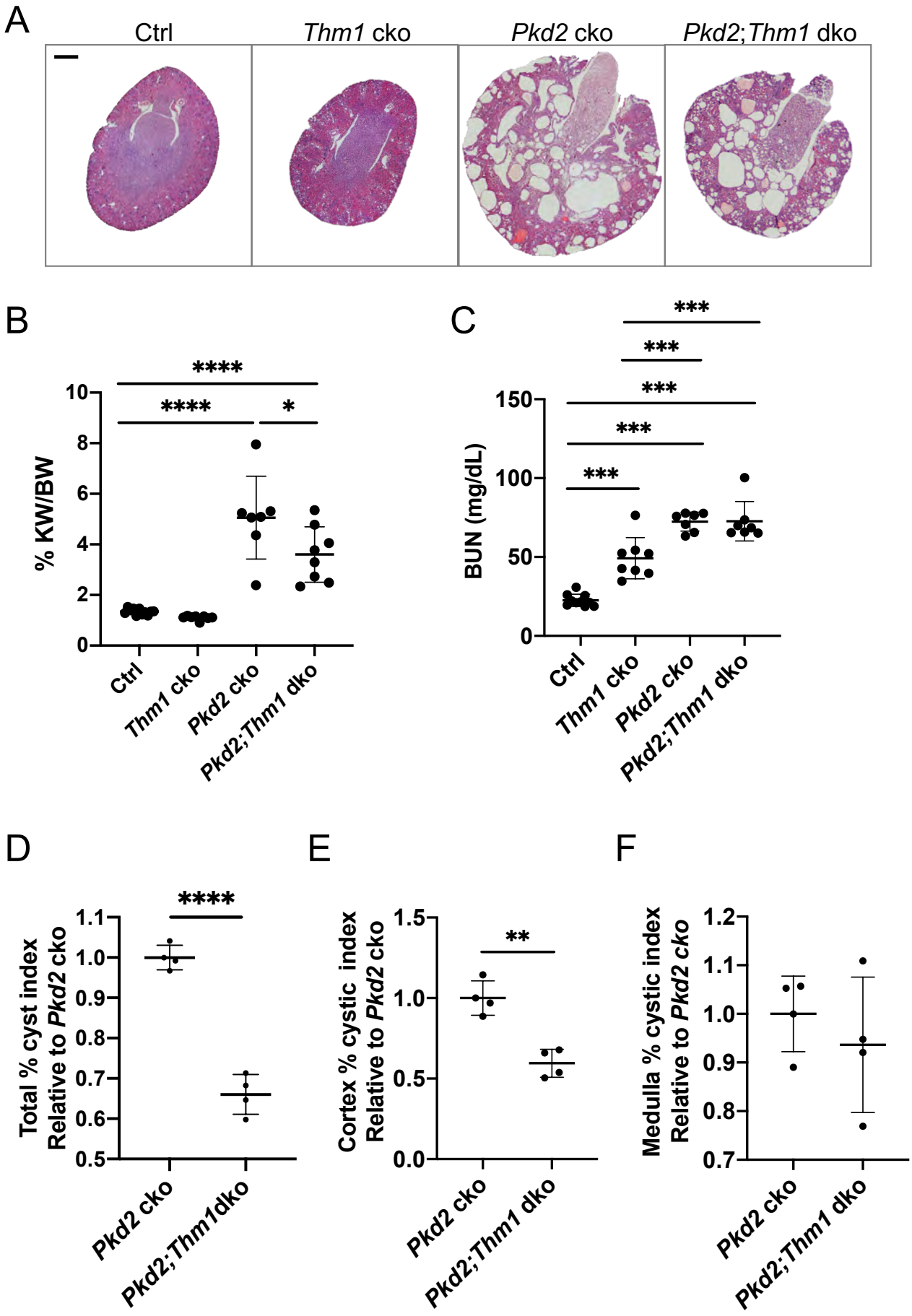

Fig 2

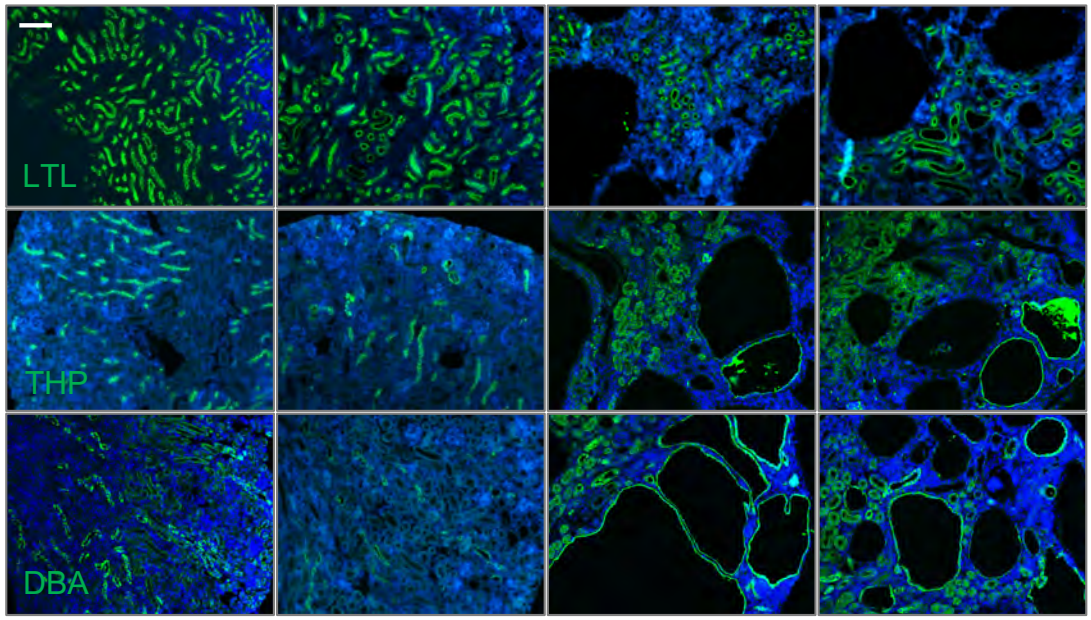

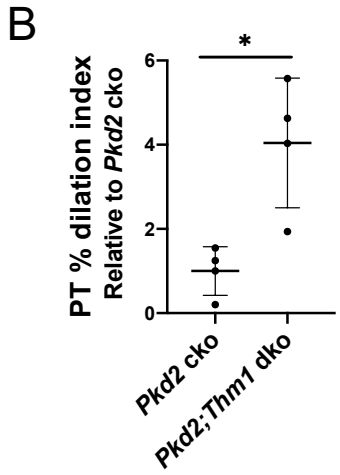

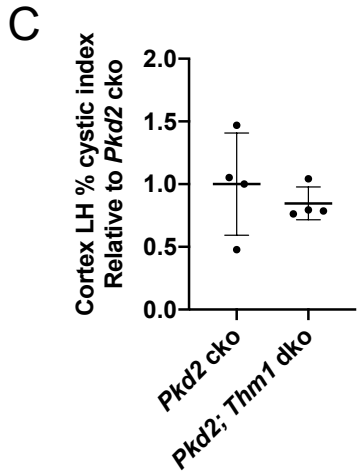

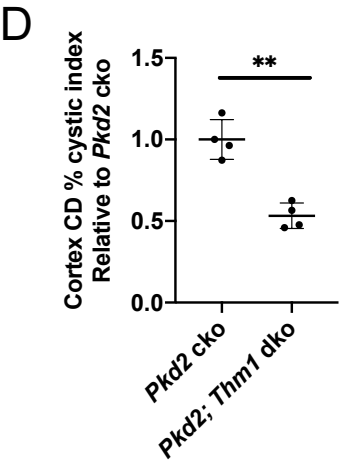

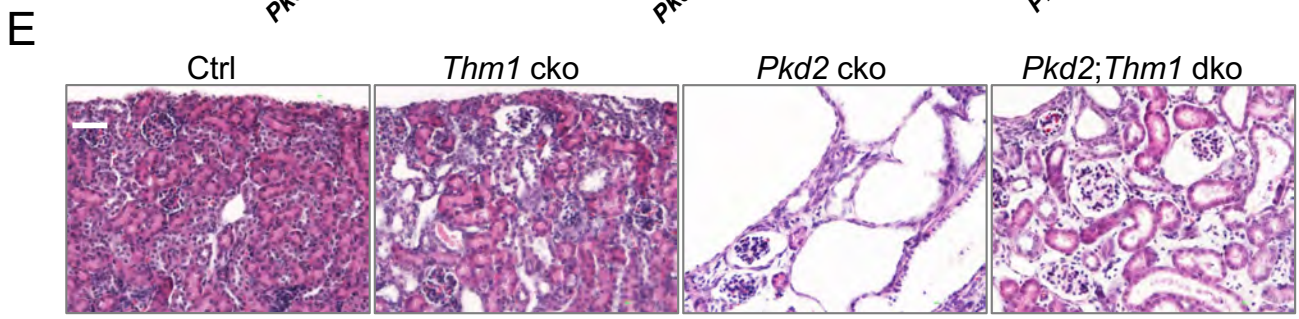

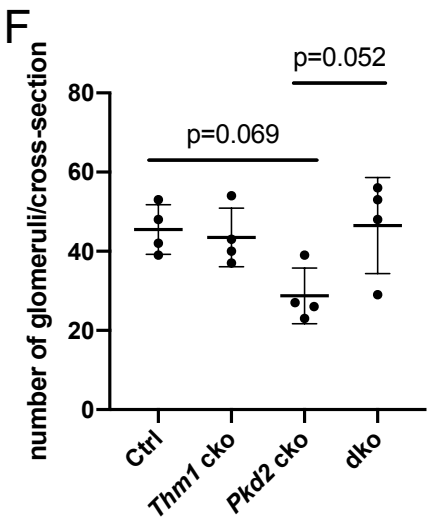

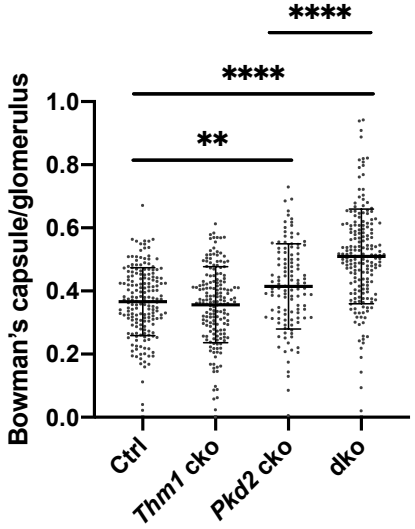

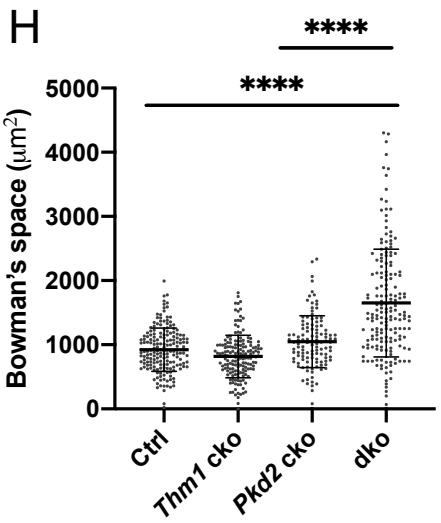

Fig 3

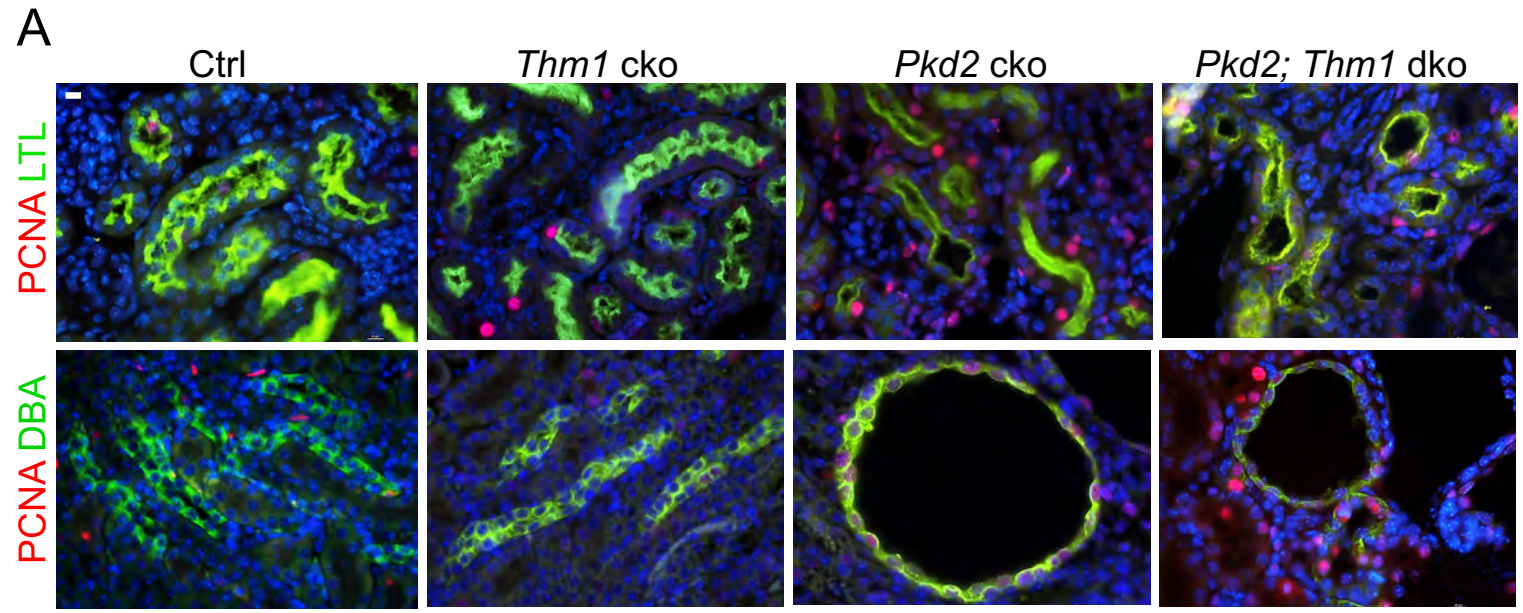

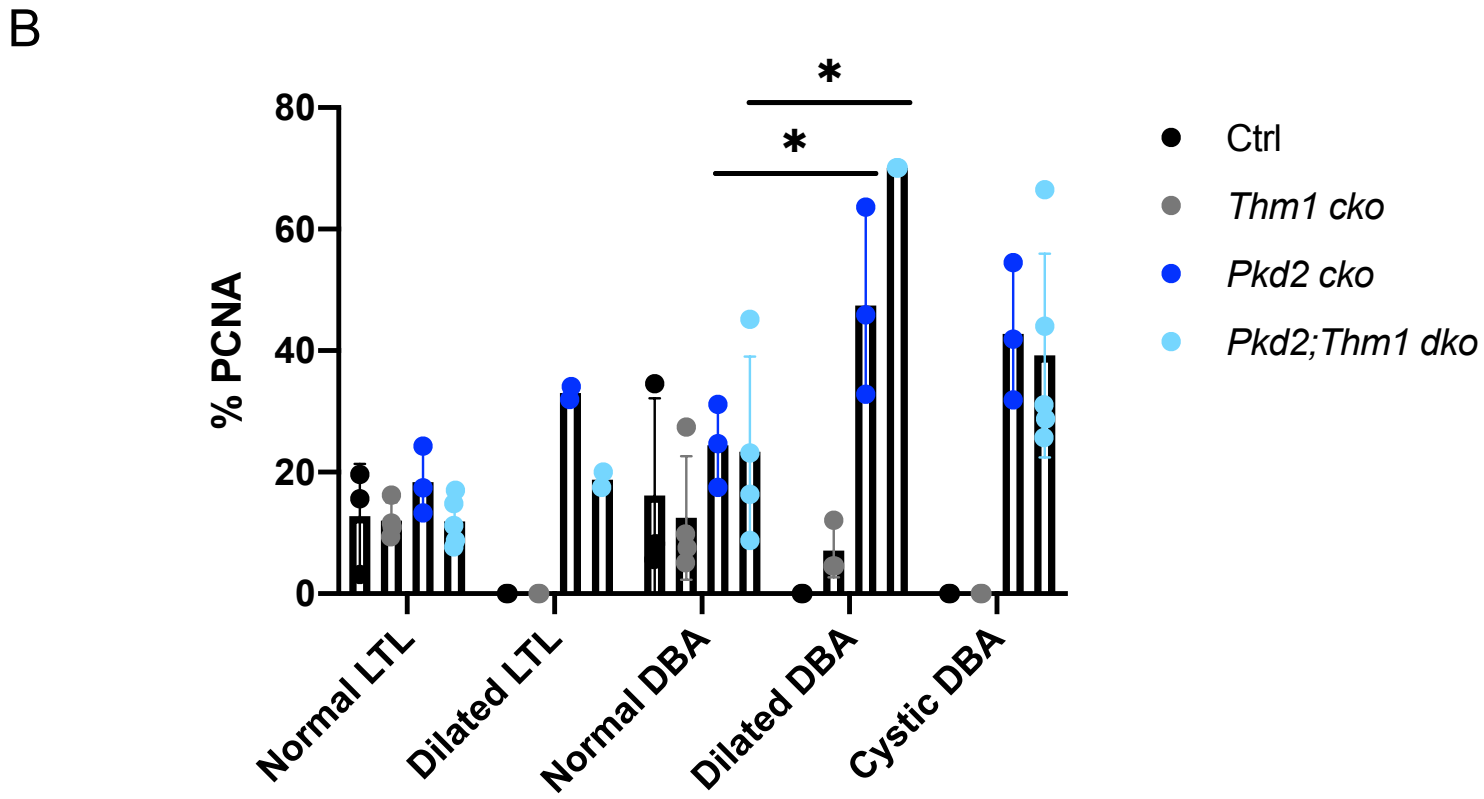

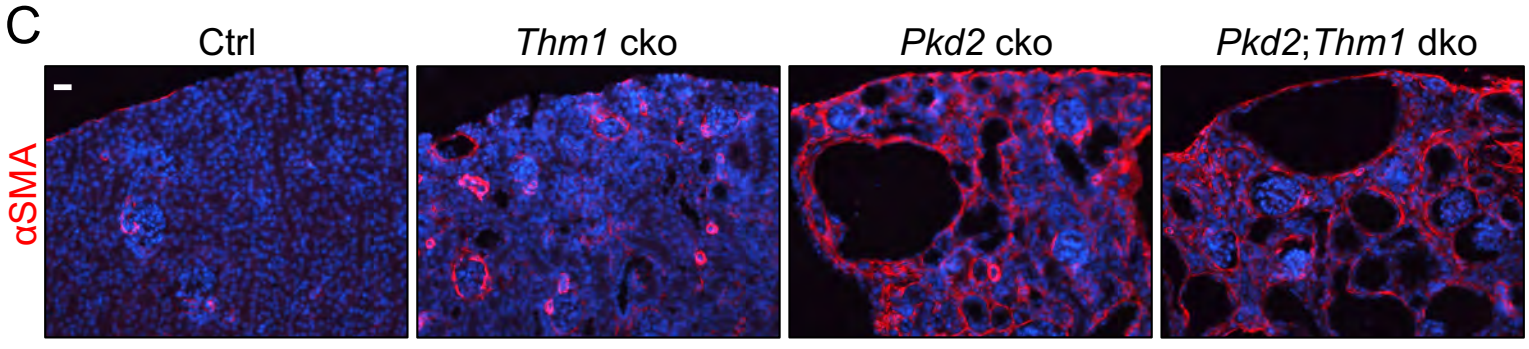

Fig 4

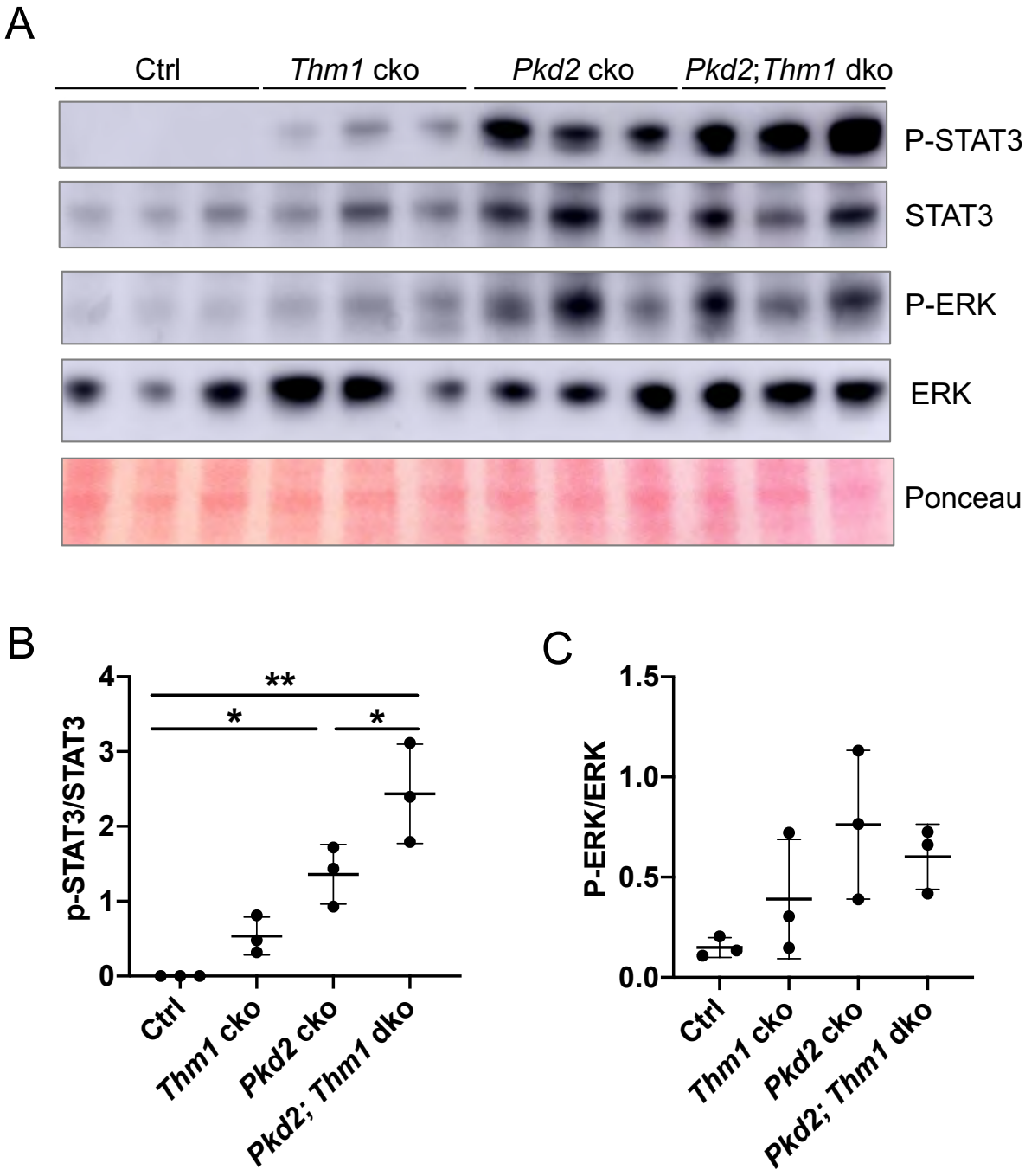

Fig 5

A

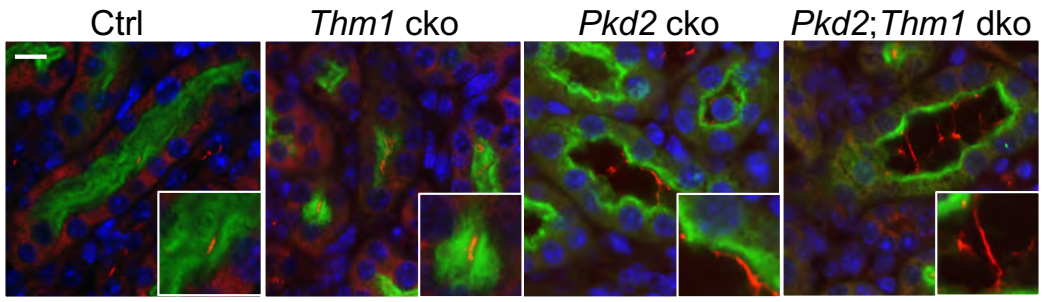

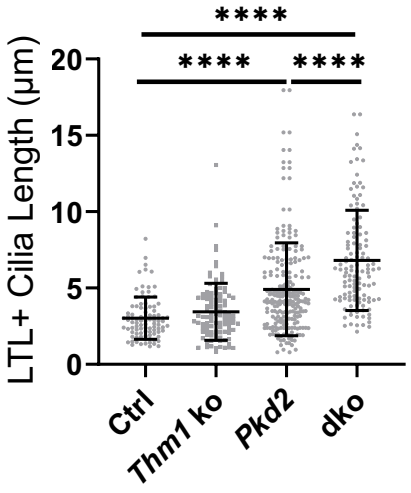

B

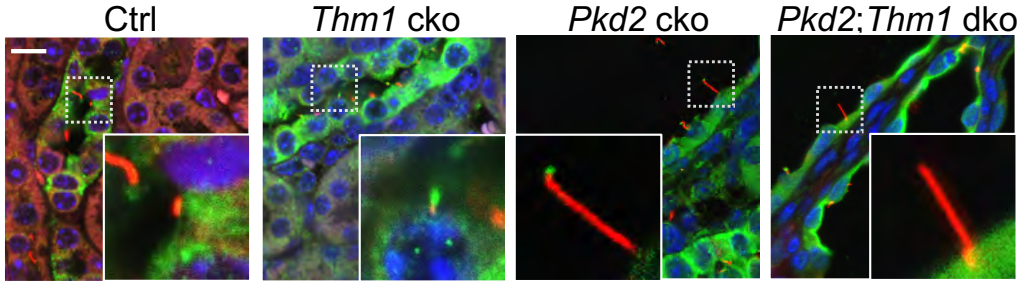

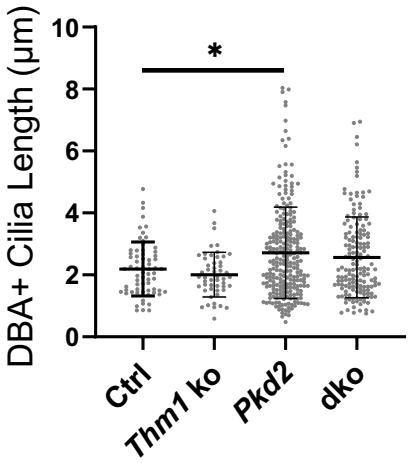

Fig 6

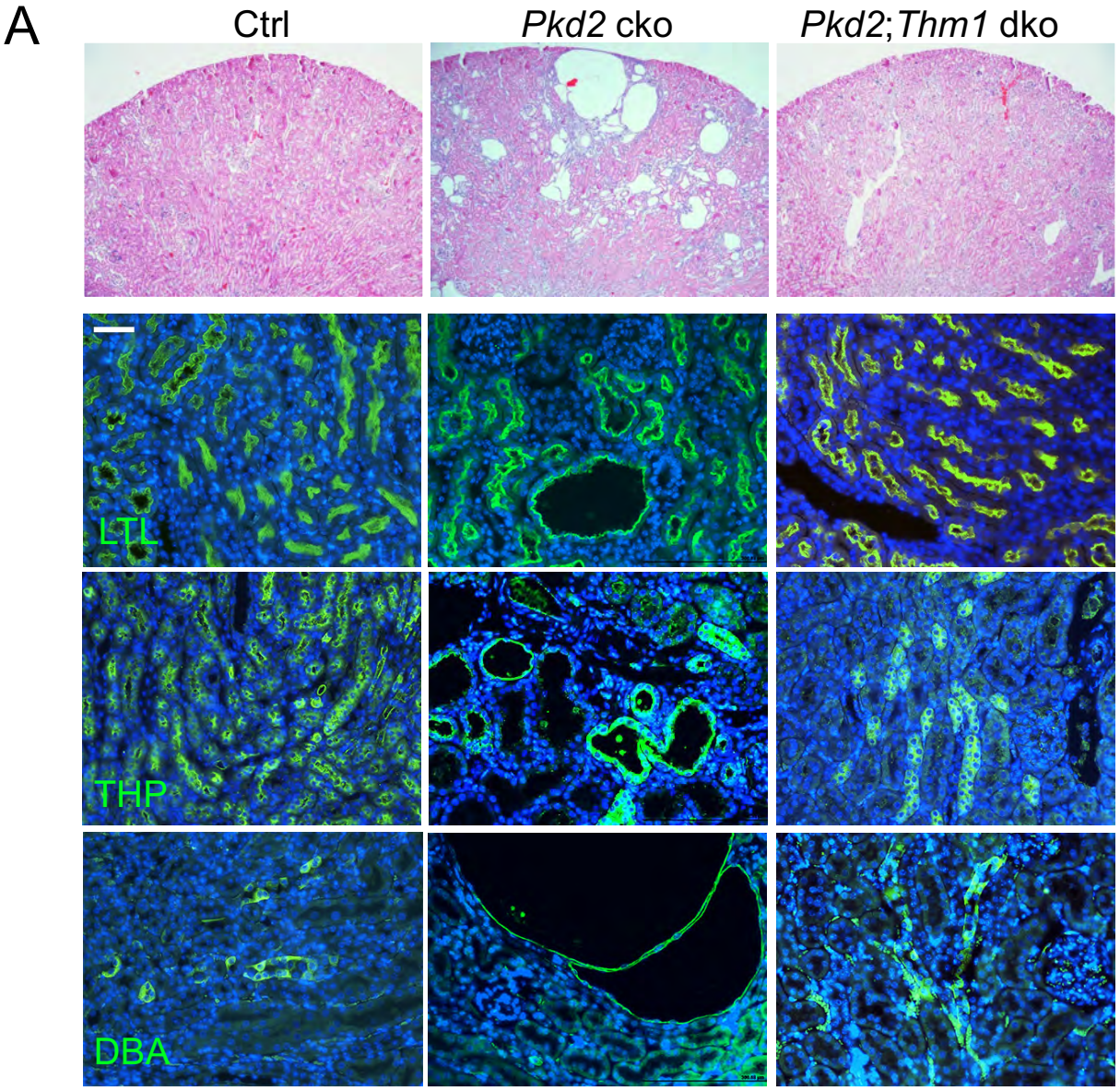

Fig 7

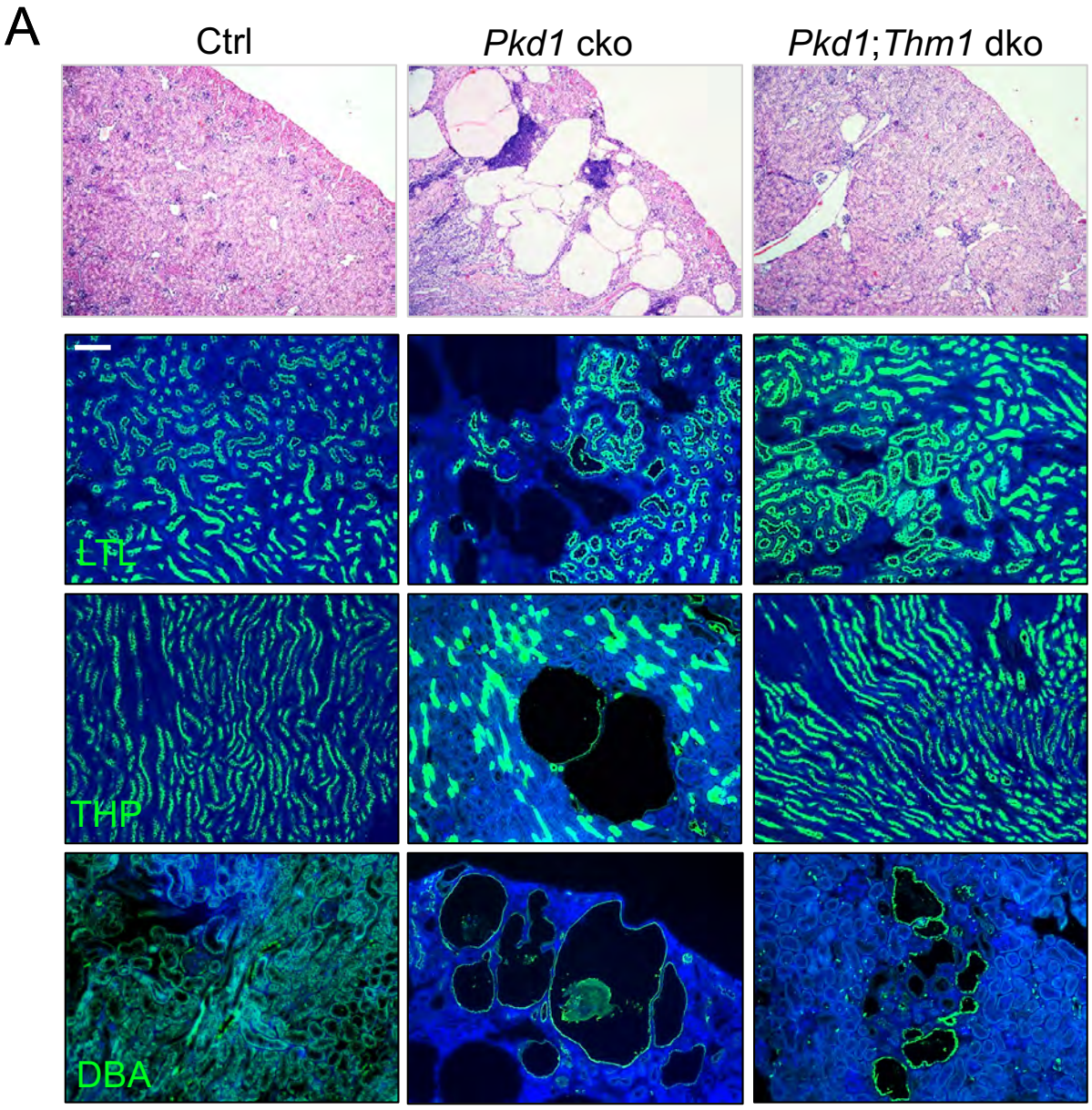

Fig 8

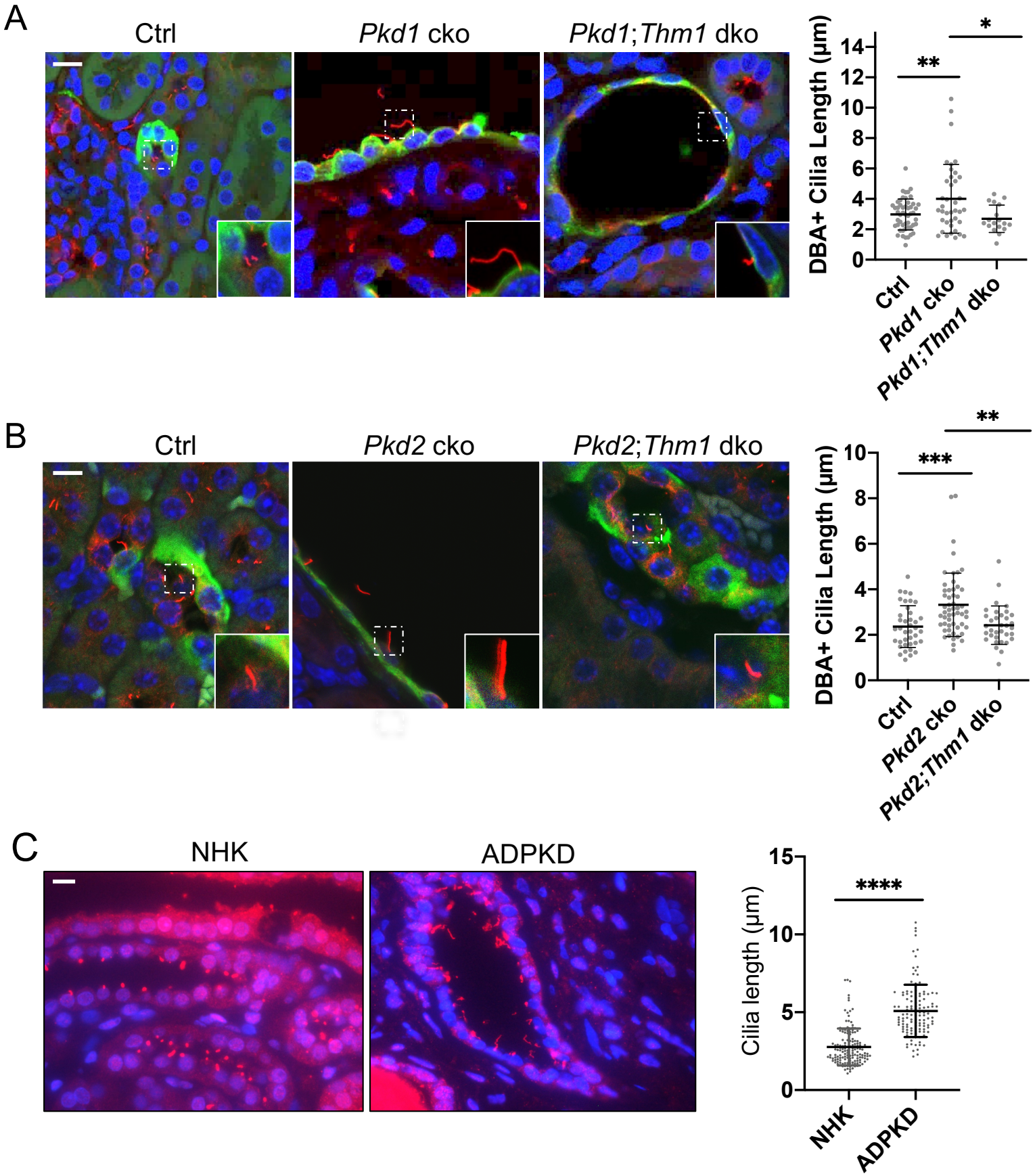
A
Ctrl
Pkd1 cko
Pkd1;Thm1 dko
DBA+ Cilia Length (μm)
0
2
4
6
8
10
12
14
**
*
Ctrl
Pkd1 cko
Pkd1;Thm1 dko
B
Ctrl
Pkd2 cko
Pkd2;Thm1 dko
DBA+ Cilia Length (μm)
0
2
4
6
8
10
***
**
Ctrl
Pkd2 cko
Pkd2;Thm1 dko
C
NHK
ADPKD
Cilia length (μm)
0
5
10
15
****
NHK
ADPKD

Intraflagellar transport-A deficiency ameliorates ADPKD renal cystogenesis in a renal tubular- and maturation-dependent manner
Wei Wang *et al*.

Supplemental Material

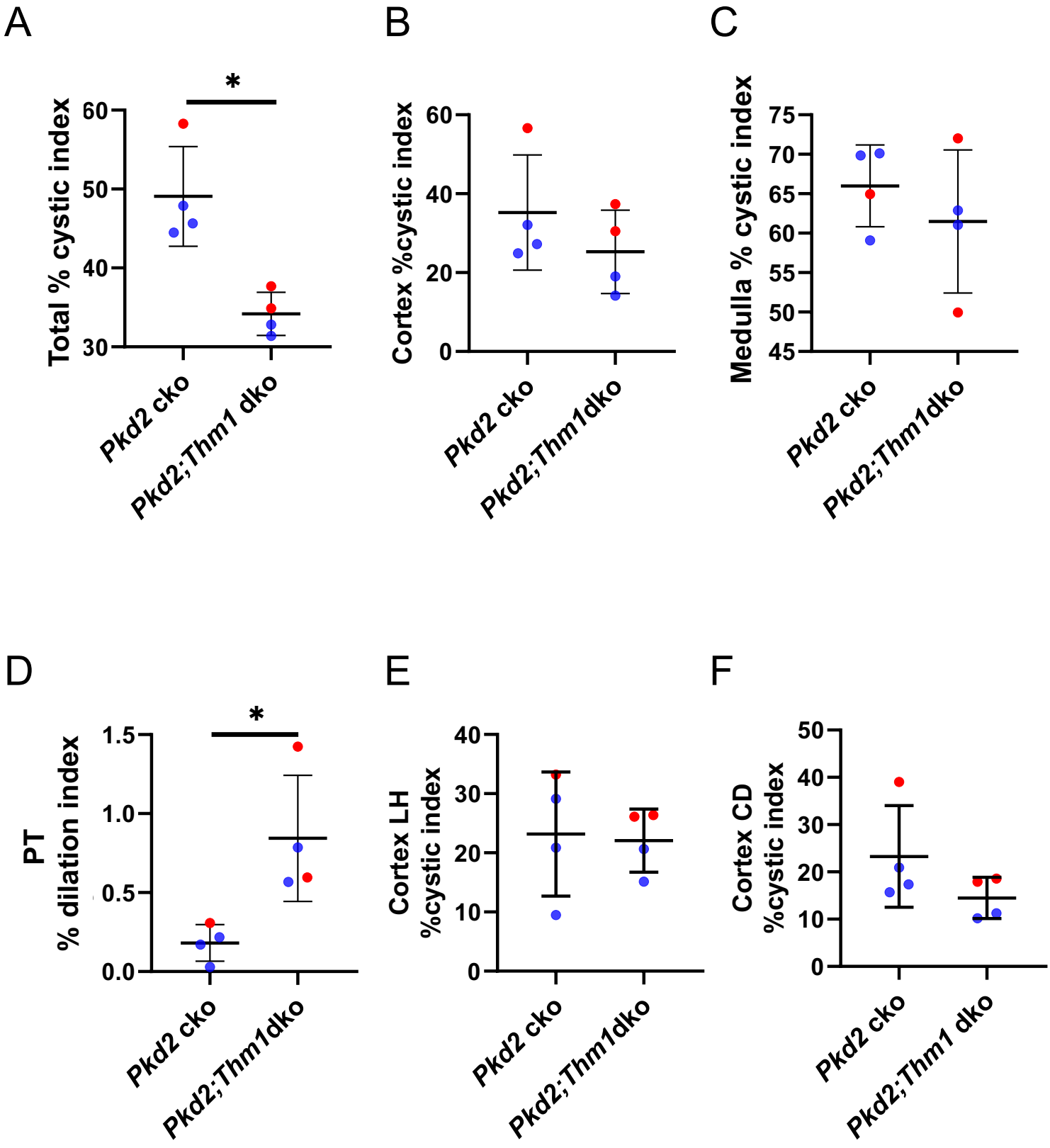

Supplementary Figure 1. Renal cystic index of early onset *Pkd2* cko mice. (A) Percent total cystic index (B) Percent cortical cystic index (C) Percent medullary cystic index (D) Percent LTL+ dilations (E) Percent THP+ cystic index (F) Percent DBA+ cystic index in renal cortex. Bars represent mean ± SD. Statistical significance was determined by unpaired two-tailed t-test. *p<0.05

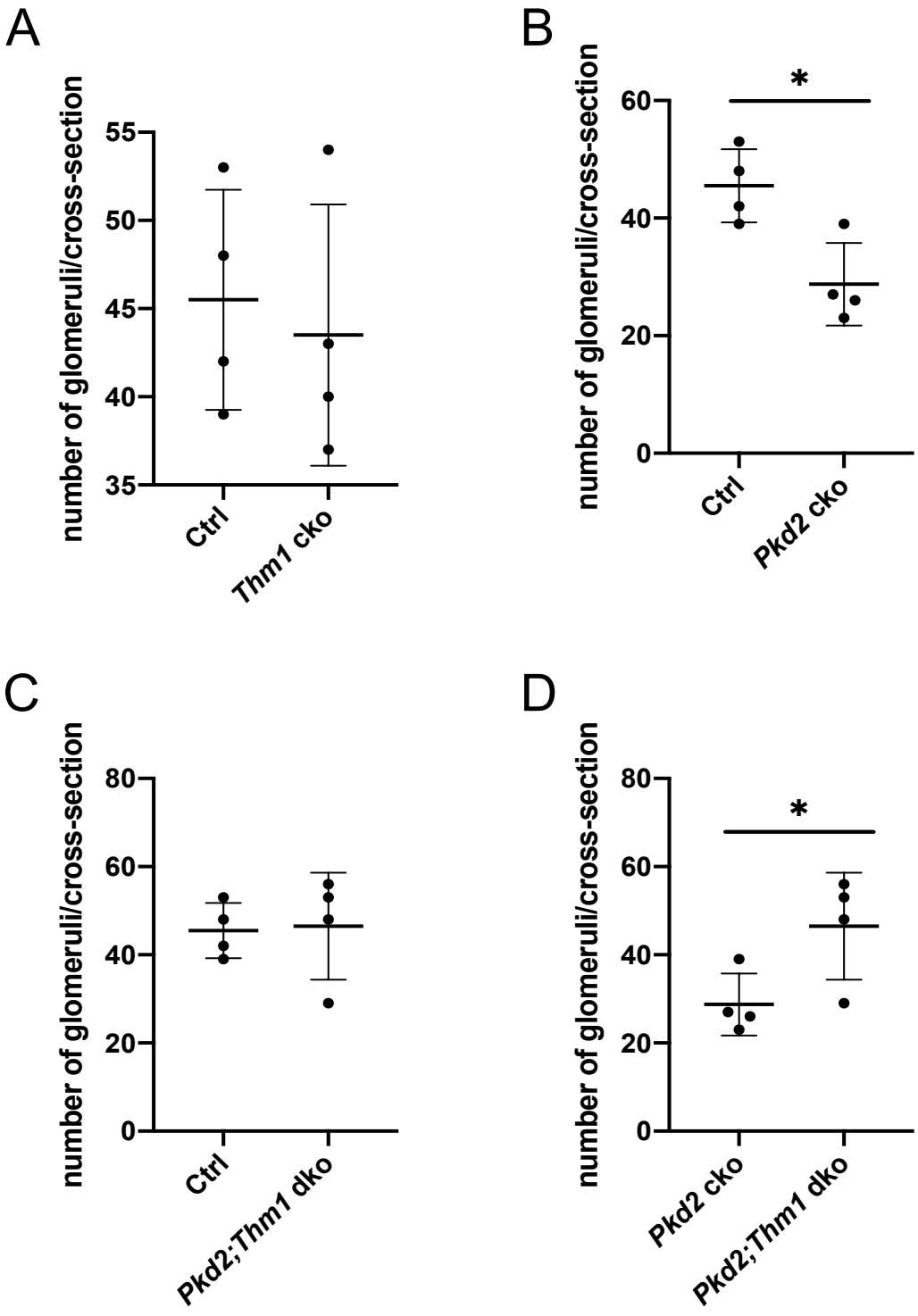

Supplementary Figure 2. Glomerular number per kidney cross-section. (A) Control vs. *Thm1* cko (B) Control vs. *Pkd2* cko (C) Control vs. *Pkd2;Thm1* dko; (D) *Pkd2* cko vs. *Pkd2;Thm1* dko. Bars represent mean ± SD. Statistical significance was determined by unpaired two-tailed t-test. *p<0.05

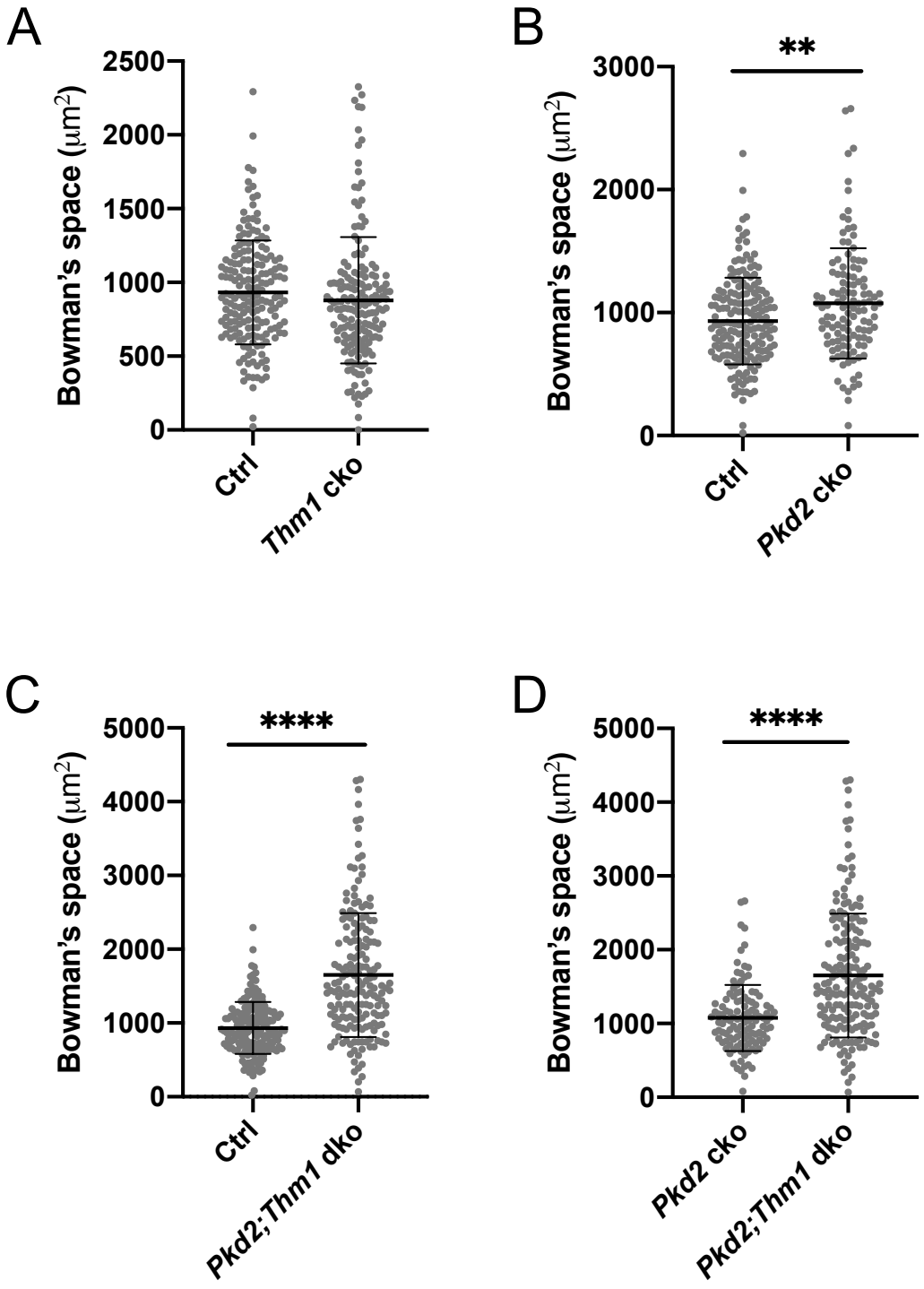

Supplementary Figure 3. Area of Bowman's space. (A) Control vs. *Thm1* cko (B) control vs. *Pkd2* cko (C) control vs. *Pkd2;Thm1* dko; (D) *Pkd2* cko vs. *Pkd2;Thm1* dko. Bars represent mean ± SD. Statistical significance was determined by unpaired two-tailed t-test. **p<0.005; ****p<0.00005

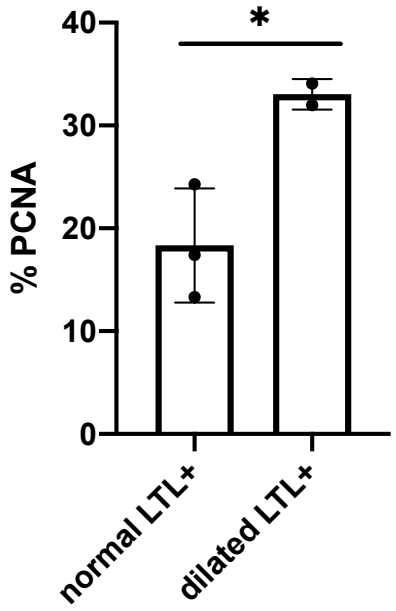

Supplementary Figure 4. Proliferation of *Pkd2* cko proximal tubular cells. Quantification of PCNA+ cells in normal and dilated LTL+ tubules of *Pkd2* cko kidneys. Bars represent mean ± SD. Statistical significance was determined by unpaired two-tailed t-test. *p<0.05

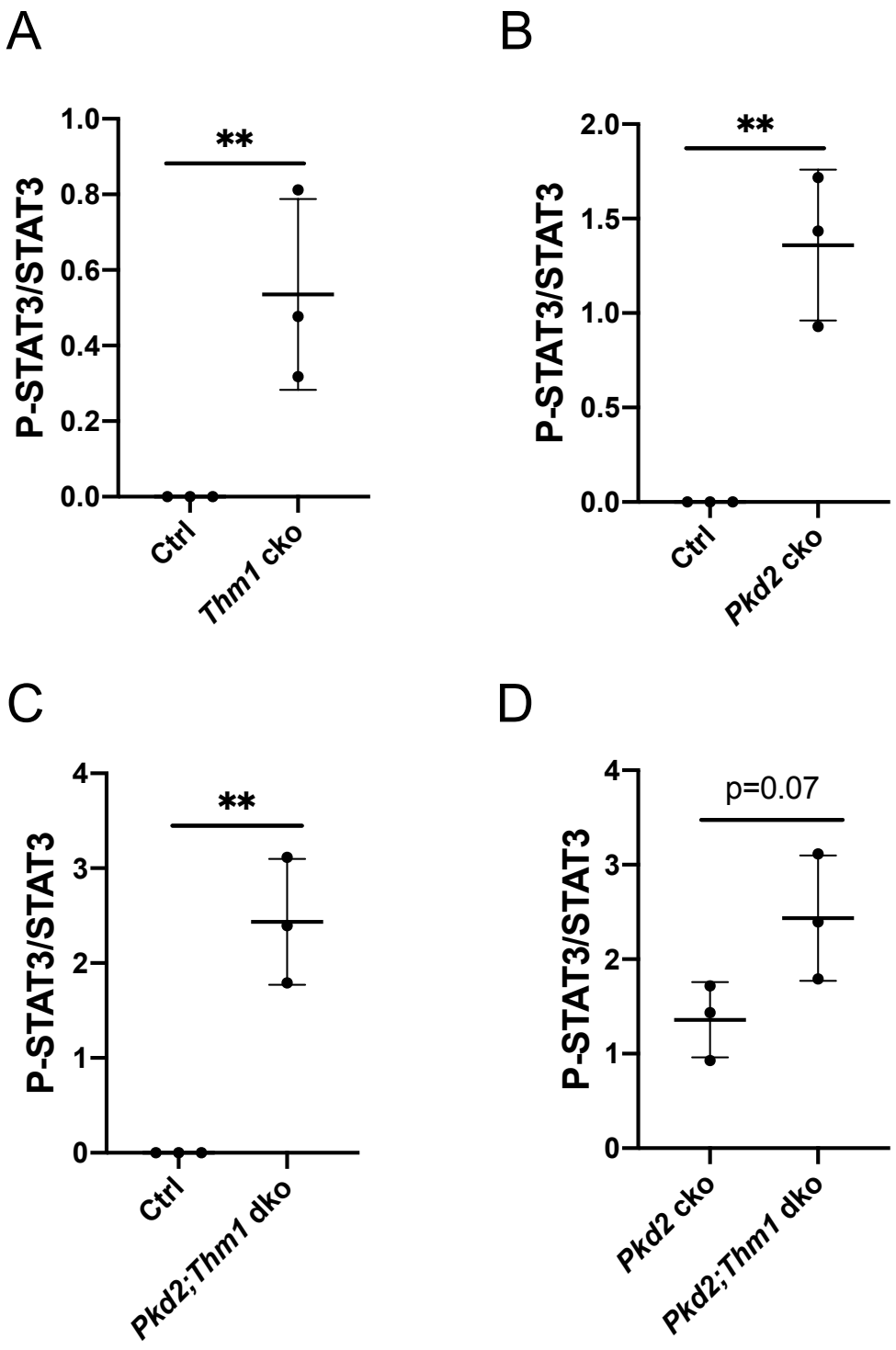

Supplementary Figure 5. Quantification of P-STAT3/STAT3 Western blot. (A) P-STAT3/STAT3 of control vs. *Thm1* cko; (B) control vs. *Pkd2* cko; (C) control vs. *Pkd2;Thm1* dko; (D) *Pkd2* cko vs. *Pkd2;Thm1* dko. Bars represent mean ± SD. Statistical significance was determined by unpaired two-tailed t-test. **p<0.005

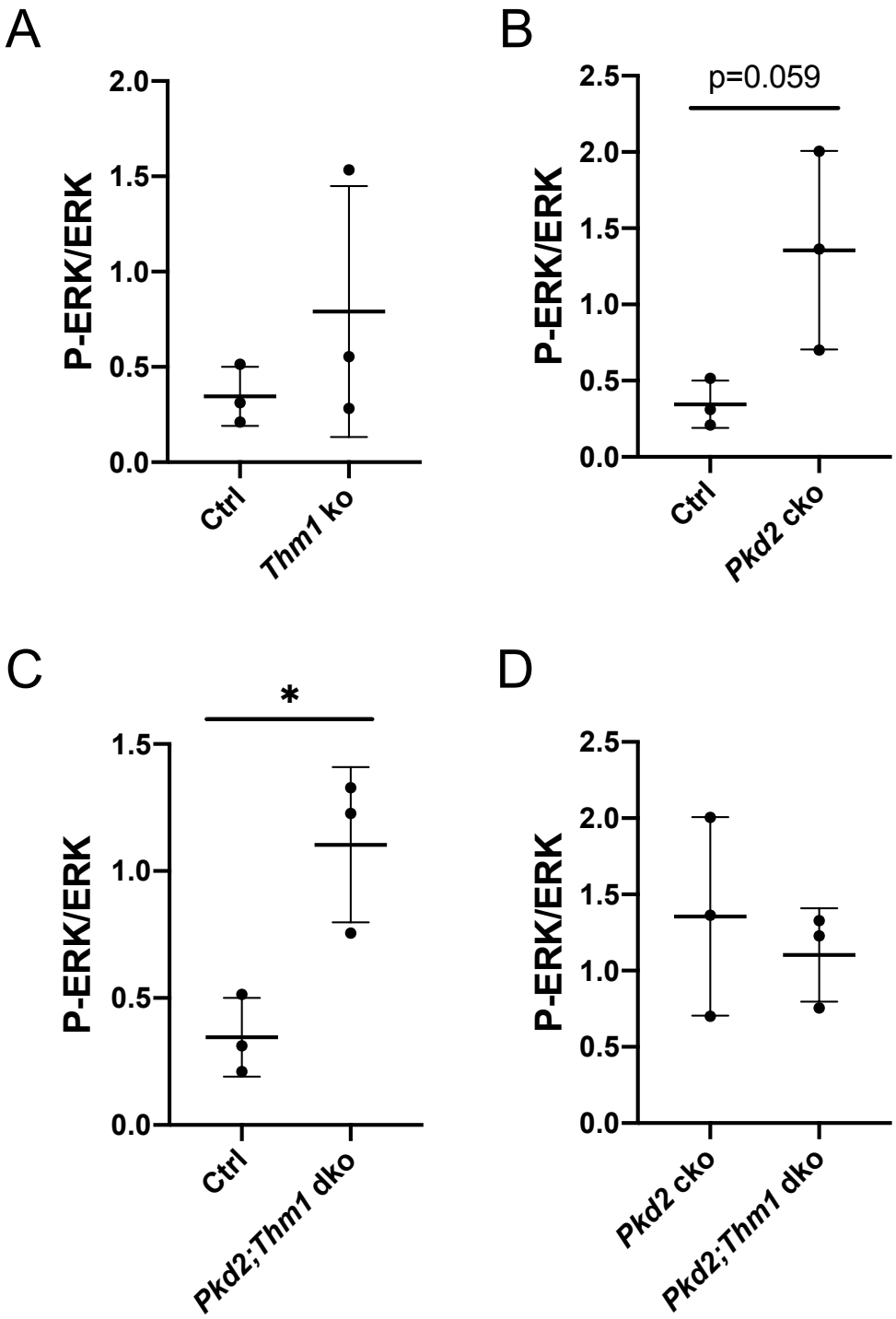

Supplementary Figure 6. Quantification of P-ERK/ERK Western blot. (A) P-ERK/ERK of control vs. *Thm1* cko; (B) control vs. *Pkd2* cko; (C) control vs. *Pkd2;Thm1* dko; (D) *Pkd2* cko vs. *Pkd2;Thm1* dko. Bars represent mean ± SD. Statistical significance was determined by unpaired two-tailed t-test. *p<0.05

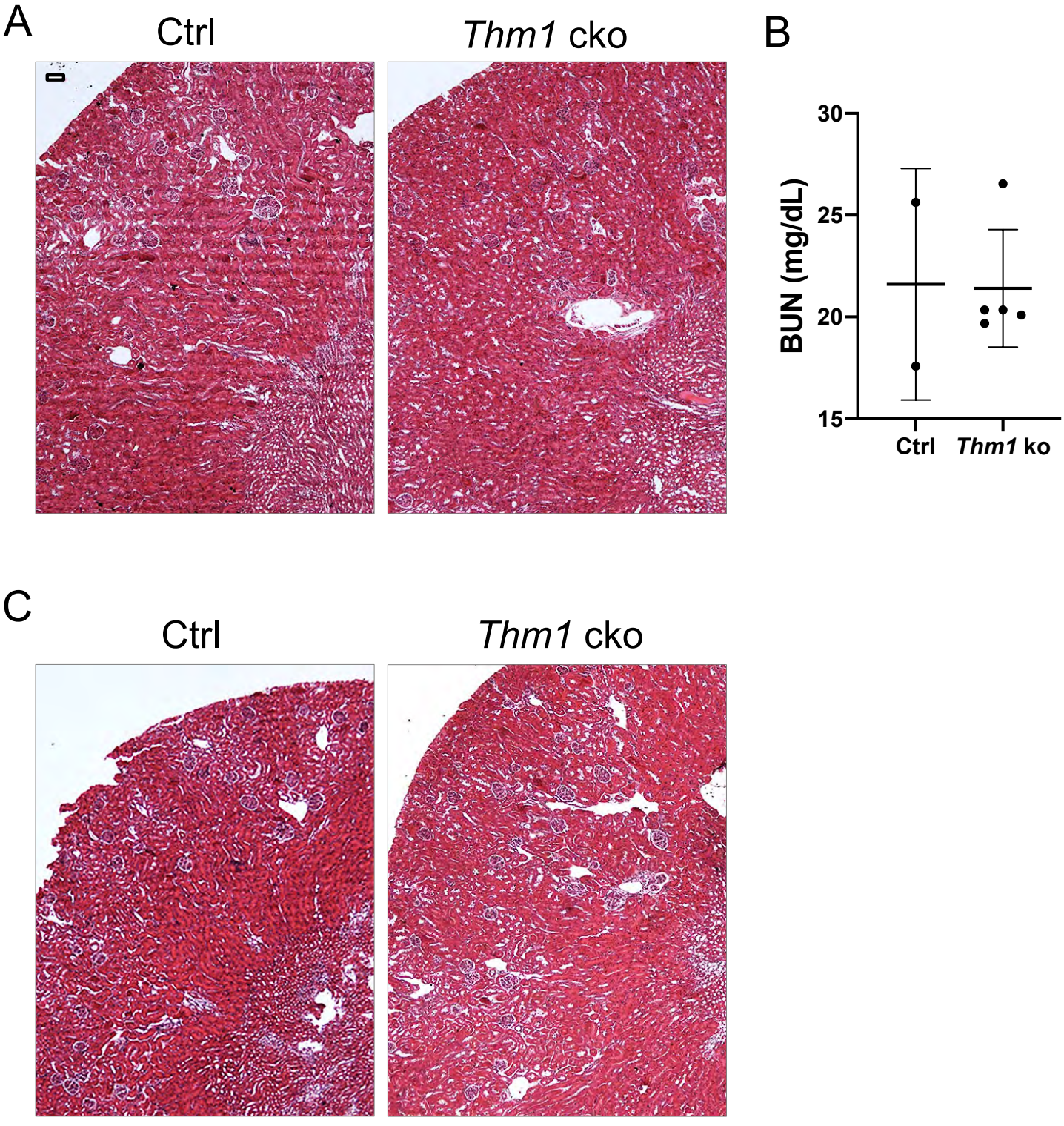

Supplementary Figure 7. Renal histology of late onset *Thm1* cko mice. (A) Haemotoxylin and eosin staining, and (B) BUN levels of 6-month-old *Thm1* cko kidneys following *Thm1* deletion at P28. Scale bar - 50μm. (C) Haemotoxylin and eosin staining of 6-month-old *Thm1* cko kidneys following *Thm1* deletion at P35.

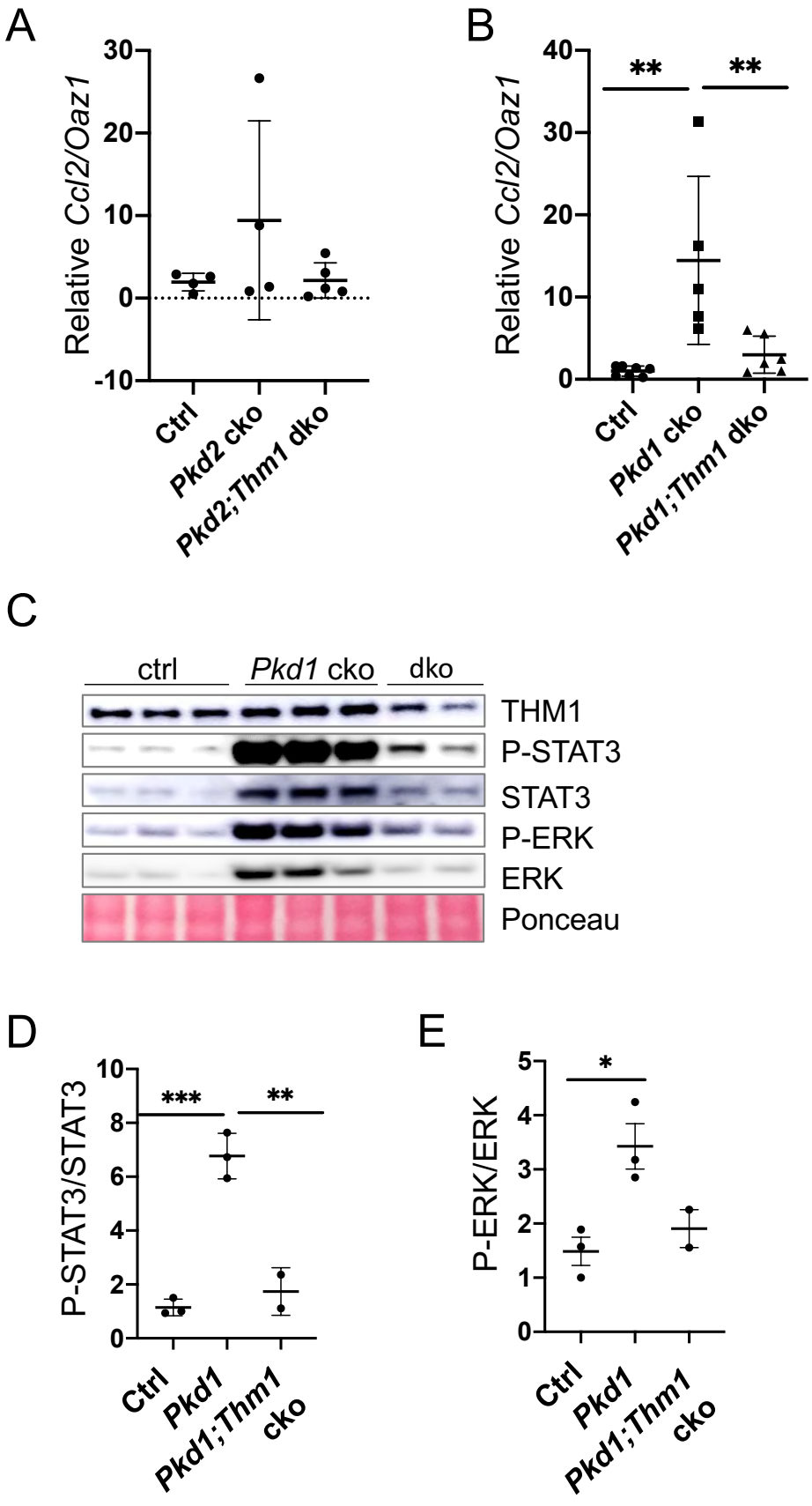

Supplementary Figure 8. *Thm1* deletion in late onset ADPKD models decreases signaling. (A) qPCR for *Ccl2* in renal extracts of *Pkd2* cko and *Pkd2;Thm1* dko mice and (B) of *Pkd1* cko and *Pkd1;Thm1* dko mice. (C) Western blot analysis of *Pkd1* cko and *Pkd1;Thm1* dko kidney extracts. (D) Quantification of P-STAT3/STAT3 and (E) P-ERK/ERK. Bars represent mean ± SD. Statistical significance was determined by one-way ANOVA followed by Tukey's test. *p<0.05; **p<0.005; ***p<0.0005